EPSC2017

SB5 abstracts

EPSC Abstracts
Vol. 11, EPSC2017-119, 2017
European Planetary Science Congress 2017

How the Distribution of Impact Ejecta may explain Surface Features on Ceres and Saturnian Satellites

N. Schmedemann(1), A. Neesemann(1), F. Schulzeck(2), K. Krohn(2), I. von der Gathen(2), K. A. Otto(2), R. Jaumann(1,2), R.Wagner(2), G. Michael(1), C. A. Raymond(3), C. T. Russell(4)
(1)Institute of Geological Sciences, Freie Universität Berlin, Berlin, Germany; (2)German Aerospace Center, Institute of Planetary Research, Berlin, Germany; (3)JPL, Caltech, Pasadena, CA, USA, (4)University of California, Los Angeles, CA, USA. (nico.schmedemann@fu-berlin.de)

Abstract

The numerical simulation of impact ejecta on Ceres shows deposition patterns in very good agreement with observed anomalies in color ratio data as well as the location and orientation of secondary crater chains. Secondary craters are also observed on the Saturnian satellites Rhea and Tethys where the same approach could help to improve the analysis of the cratering records.

1. Introduction

Since March 6 2015 the Dawn spacecraft [1] has been in orbit around the dwarf planet Ceres. High resolution global mapping with its Framing Camera (FC) [2] revealed a much more densely cratered surface than expected [3]. At small (< 10 km) crater diameters Ceres appears to be peppered with secondary craters that often align in chains or form clusters. Some of such possible crater chains follow curved geometries and are not in a radial orientation with respect to possible source craters [4]. Ceres is a fast rotating body (~9 h per revolution) with comparatively low surface gravity (~0.27 m/s²). Thus, the distribution pattern of the back-falling ejected material is heavily affected by Coriolis forces that results in a highly asymmetrical and curved pattern of secondary crater chains.

2. The Model

In order to simulate flight trajectories and the distribution of impact ejected material for individual craters on Ceres we used the scaling laws by [5] adjusted to the Cerean impact conditions, the impact ejecta model by [6] and for more sophisticated simulations regarding the ejection angles the modified Maxwell Z-model by [7]. These models provide the starting conditions for tracer particles in the simulation. The trajectories of the particles are computed as n-body simulation. The simulation calculates the positions and impact velocities of each impacting tracer particle with respect to the rotating surface of Ceres, which is approximated by a two-axis ellipsoid. Since high and far flying particles reach significant fractions of the escape velocity, disturbing gravitational forces by the Sun and the major planets are also taken into account. In the model we assume an impact with an angle of 45 degrees and a symmetric geometry for the ejected particles. The scaling parameters for the projectile-crater size conversion are given in [8] (LDM model). The more simplistic model further assumes that all particles are ejected at a fixed angle with the local surface (in general 45°). All particles that are ejected at lower velocities than 150 m/s are neglected, because they are deposited fairly symmetrical around the source crater (continuous ejecta) but due to the high number of particles take most of the computing time. The value of 150 m/s is chosen because this might be the lower limit for forming secondary craters [9].

3. Results

Initial results of the more simplistic model show a number of interesting features in the deposition geometries of specific craters that are roughly in agreement with features that can be observed in FC imaging data of the Cerean surface. Fast jets that leave the source crater at low ejection angles appear to form systems of rays around fresh impact craters. In the case of Occator one of such rays can be mapped half way around the circumference of Ceres in color ratio data. Our ejecta model is able to reproduce this feature if a narrow beam of particles is assumed to leave Occator crater at a shallow angle of 10° w.r.t. the local surface at an azimuth of 256° (Figure 1, top and middle panel). Areas of high tracer particle density of the Urvara impact coincide with observed crater chains that are not in a radial

orientation to any nearby crater (Figure 1, bottom panel). Particles that are ejected faster than a certain velocity into the rotation direction of Ceres are overtaken by the rotation of Ceres during their flight. This effect is causing a slowing down of the eastward propagation speed of the back-falling ejecta curtain and eventually the direction is reversed, such that eastward-ejected particles are falling back into and west of the source crater. For the case of the Urvara impact the curved geometry of the border line where the ejecta curtain changed its propagation direction can be identified in color ratio data (Figure 1, top and bottom panel). The higher color ratio closer to Urvara further indicates a relatively young age for the ejecta deposition time [10]. For the Saturnian satellite Tethys we find good agreement with Telemachus' secondary crater chains south-west of the Odysseus basin, which cross-cut Odysseus secondary crater chains.

4. Conclusions

Our ejecta simulation is able to give reasonably good indication of how specific features in color ratio data and certain crater chains might have formed. The simulations are primarily visualizing the probability for secondary cratering and ejecta accumulations by the spatial density distribution of tracer particles pictured by kernel density maps (Figure 1, bottom panel). The ejected volume of specific craters is limited. Thus, individual tracer particles are not representative for individual secondary projectiles or craters. In this study, we model symmetric ejection geometries at fixed ejection angles in order to understand the basic effects of high Coriolis forces. The more sophisticated modified Maxwell Z-model can be used in future work for simulating oblique impacts causing asymmetric ejection geometries.

Acknowledgements

This work has been supported by the German Space Agency (DLR) on behalf of the Federal Ministry for Economic Affairs and Energy, Germany, grants 50 OW 1505 (NS, AN), 50 OH 1503 (NS) and 50 QM 1301 (GM), and Helmholtz-Gemeinschaft (Helmholtz Association) PD-207 (KK). We thank the Dawn flight team for their excellent job of navigating and maintaining the probe.

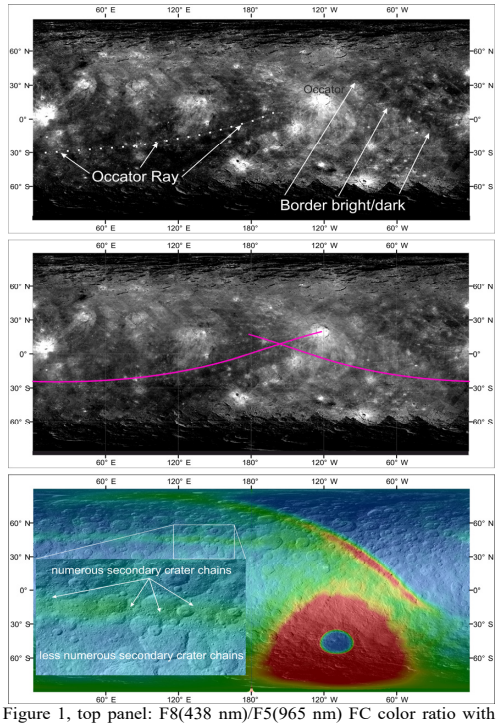

Figure 1, top panel: F8(438 nm)/F5(965 nm) FC color ratio with marked ray of Occator crater and a border between high/low color ratio. Middle panel: Trajectory of tracer particles that are ejected from Occator at 10° angle with the local surface and 256° azimuth with velocities of ≤ 510 m/s. Bottom panel: Kernel density map of the positions where tracer particles reimpacted on the surface after they were ejected during the Urvara impact. Colors indicate the relative particle density from low (blue) to high (red). The inlay shows a magnified clear filter version of the boxed area. The inlay confirms several E-W oriented crater chains where the kernel density map also indicates an E-W oriented narrow band of increased tracer particle density. The dark/bright boundary from top panel is coinciding with high densities of eastward-ejected particles.

References

[1] Russell C. T. et al.: *Science*, 353, 1008 (2016). [2] Sierks H. et al.: *Space Science Reviews*, 163, 263 (2011). [3] Bland M. T. et al.: *Nature Geoscience*, 9, 538 (2016). [4] Scully J. E. C. et al.: *American Astronomical Society, DPS meeting #48*, id.321.02 (2016), Pasadena, USA. [5]. Ivanov B. A.: *Space Science Reviews*, 96, 87 (2001). [6] Housen K. R. and Holsapple K. A.: *Icarus*, 211, 856 (2011). [7] Anderson J. L. B. et al.: *Meteoritics and Planetary Science*, 39, 303 (2004). [8] Hiesinger H. et al.: *Science*, 353, 1003 (2016). [9] Bierhaus E. B. et al.: *Icarus*, 218, 602 (2012). [10] Schmedemann N. et al.: *GRL*, 43, 11987 (2016).

EPSC Abstracts
Vol. 11, EPSC2017-176, 2017
European Planetary Science Congress 2017

DAWN FC Results at Vesta and Ceres

A. Nathues (1), M. Hoffmann (1), G. Thangjam (1), T. Platz (1), H. Sierks (1), U. Christensen (1), L. Le Corre (2/1), V. Reddy (3/1), C. T. Russell (4), C. Raymond (5), K. Mengel (6) and the Dawn Science Team (1) MPI for Solar System Research, Göttingen, Germany, (nathues@mps.mpg.de, +49 551 384 979 433), (2) Planetary Science Institute, Tucson, USA, (3) Lunar and Planetary Laboratory, University of Arizona, Tucson AZ, USA, (4) University of California, Institute of Geophysics, Los Angeles, USA; (5) Jet Propulsion Laboratory, Pasadena, USA, (6) Clausthal University of Technology, Clausthal-Zellerfeld, Germany

1. Introduction

Dawn, the first spacecraft orbiting successively two planetary bodies beyond the Earth environment, has returned a wealth of information about the first two massive asteroids (4) Vesta and (1) Ceres. Both differ by a factor of two in size [1], and in their location in the asteroid belt, being separated by the snow-line [2]. While previous ground-based observations identified several key properties [3, 4], the detailed exploration of these objects, spatially and spectrally well resolved information on mineralogy and geology, had been left for Dawn. The spacecraft has orbited Vesta 2011-2012, and Ceres from 2015 onwards.

2. Results

Collisional history has led to a bare escape of destruction for Vesta but only to some major basins on Ceres. Their difference in material density reflects different compositions. While Vesta is a fully differentiated [5], igneous body, Ceres' primitive crust is consistent with an incomplete differentiation [6], a fact also confirmed by Dawn. These constitutional differences imply different histories of accretion. Vesta's violent collisional history has led to a widespread deep regolith [7], unprecedented elsewhere in the solar system. That Ceres is very different in this respect is consistent with its different composition and thermal history. Vesta's surface is characterized by basaltic and gabbroic rocks, i.e., by HED lithology [8]. However, the expected content of olivine turned out to be restricted to almost negligible parts of the surface and to an exogenic origin of the olivine [9]. On the other hand, the presence of dark carbonaceous impactor material, which even delivered hydrated minerals to Vesta's surface, was another major surprise [10]. On the contrary, several expectations about the surface composition of Ceres could be confirmed, but the way these are represented, had not been expected. The most obvious new findings are the substantial proportion of carbonates in its surface materials [11], and their concentration associated with very young impact craters, where they are exposed in high albedo areas termed "faculae" [12, 13]. The data indicate still ongoing sublimation of hydrous components including water-ice [13, 14]. Despite the remarkable findings and already performed analysis, there are still many issues that need to be resolved. For example, the enigmatic orange materials seen in global colour mosaic of Vesta (Fig. 1) and the unique red materials on Ceres are of the prioritized issues. On Ceres, it indicates the presence of aliphatic organic material [15] whose distribution hints at an exogenous origin [18]. The orange material on Vesta comes in at least two varieties whose origin is not understood yet uniquely [16]. Dawn FC imagery led to the discovery of many unusual surface features on Ceres and Vesta. Both asteroids have been globally mapped in seven colours and one clear filter [17, 18].

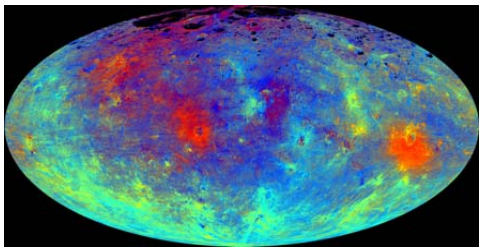

Figure 1: *Global color mosaic of Vesta (R = 0.75/0.44 µm, G = 0.75/0.92 µm, B = 0.44/0.75 µm).*

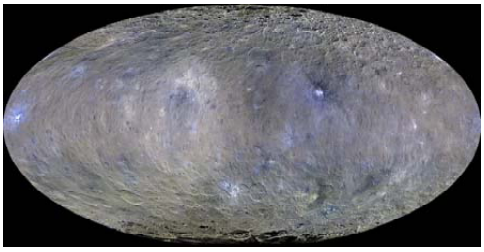

Figure 2: *Global color mosaic of Ceres (R = 0.96 µm, G = 0.75 µm, and B = 0.44 µm).*

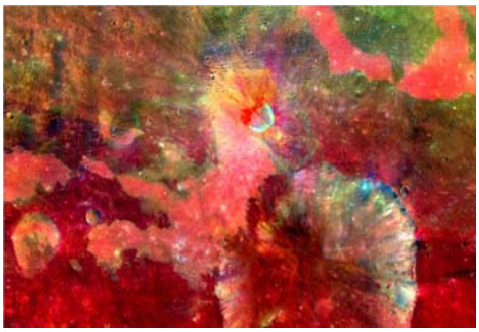

Figure 3: *Vesta's Oppia crater with potential impact melt-related materials (orange patches).*

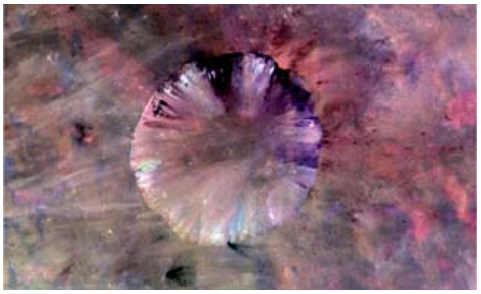

Figure 4: *Remarkable green-red transitions in a narrow putative impact generated melt flow on the western inner wall of crater Numisia on Vesta.*

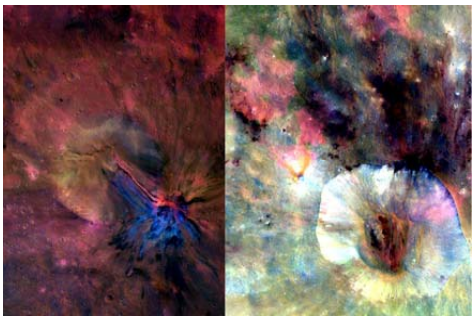

Figure 5: *Craters with complex distribution of potential melt-related and other unique features on Vesta. Aelia (left) and Drusilia (right).*

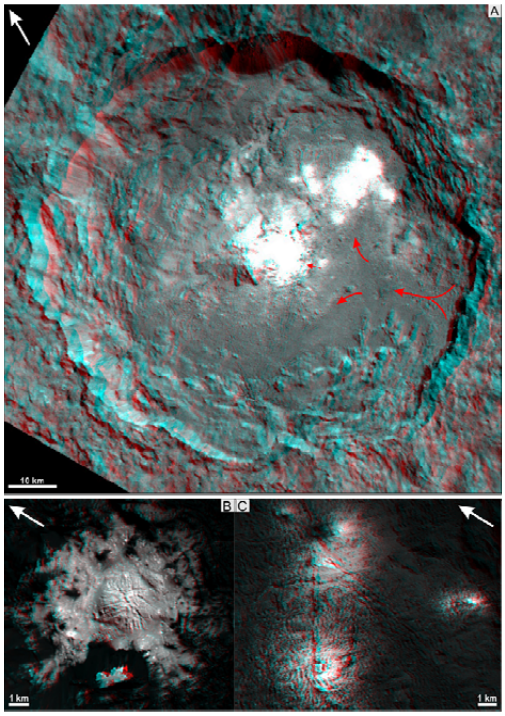

Figure 6: Occator crater on Ceres in 3D. (A) Entire crater, (B) Central pit and dome (Cerealia Facula), (C) *Vinalia Facula.*

References

[1] Morrison, D.: Geophys. Res Lett. 3, 701-704, 1976; [2] Cyr et al., K. E.:, Icarus 135, 537-548, 1998; [3] Keil, K.: Asteroids III, 573-584, 2002; [4] Neumann, W., et al., Earth Planet. Sci. Lett. 395, 267-280, 2014.; [5] McCord, T. B. et al., LPSC 48, 1098, 2017; [6] Park R. S., et al., Nature 537, 515-517, 2016; [7] Denevi, B. W., et al., Meteor. Planet. Sci. 51, 2366-2386, 2016; [8] Thangjam, G. S., et al., Meteor. Planet. Sci. 48, 2199-2210, 2013; [9] Nathues, A., et al., Icarus 258, 467-482, 2015; [10] De Sanctis , M. C., et al., Astrophys. J. 758, L36, 1-5, 2012; [11] De Sanctis, M. C., et al., Nature 536, 54-57, 2016; [12] Stein, N., et al., LPSC 48, 2547 (2017); [13] Nathues, A., et al., Nature 528, 237-240, 2015; [14] Thangjam et al., Astrophys J. 833, L25, 2017; [15] De Sanctis, M. C., et al., Science 335, 719-722, 2017; [16] Le Corre, L., et al., Icarus 226, 1568-1594, 2013; [17] Reddy, V., et al., Science 336, 700-704, 2011; [18] Nathues, A., et al., Planet. Sp. Sci. 134, 122-127, 2016.

EPSC Abstracts
Vol. 11, EPSC2017-197, 2017
European Planetary Science Congress 2017

How is water vapour released from Ceres?

M. Küppers, L. O'Rourke
ESA/ESAC, Villanueva de la Cañada, Spain (michael.kueppers@sciops.esa.int)

Abstract

Remote observations from ground and space and in-situ exploration by the Dawn spacecraft have revealed a transient water exosphere around dwarf planet (1) Ceres, demonstrating that water ice is ubiquitous in the outer asteroid belt. However, no clear conclusion has been reached about the process that drives the release of water vapour from the surface or subsurface of Ceres. We will summarize the available evidence and estimate the contribution from various suggested processes.

1. Introduction

Indirect evidence through its shape and density pointed to Ceres being differentiated into a silicate core and an icy mantel [1]. The first tentative detection of water vapour from Ceres was reported in 1992 based on IUE observations [2], and a clear signal was observed on 3 out of 4 occasions by Herschel [3]. However, not all observations resulted in water detection (see Fig. 1).

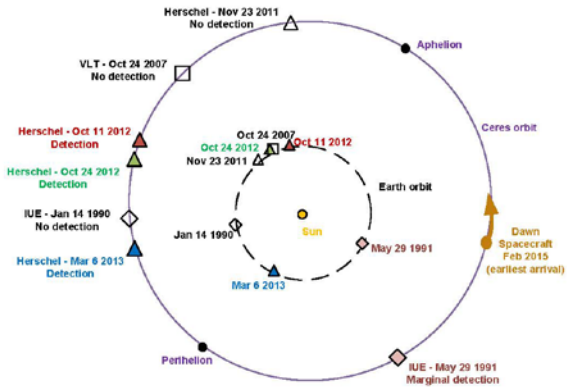

Figure 1: Observations of water vapour at Ceres before arrival of the DAWN spacecraft. Filled symbols are detections, empty symbols represent non-detections. Figure taken from [3].

The rendezvous of the Dawn spacecraft with Ceres observed the exosphere indirectly through bursts of energetic electrons, indicating the presence of a bow shock caused by an exosphere [4]. The Dawn observations confirmed the transient nature of the atmosphere. Furthermore, Dawn detected water ice on and below Ceres' surface. Now, with the Dawn mission coming to its end, it is timely to review our knowledge about water on Ceres and the mechanism of water vapour release.

2. Properties of water on Ceres

The process(es) responsible for water vapour release from Ceres need to be consistent with the following observations:

1. Near-Infrared spectra of the surface show evidence for water ice at a single near-equatorial location [5]. Water ice is more abundant in shadowed polar regions [6], but the detectable amount of surface ice is too low to explain the observed water vapour.

2. A water-rich subsurface layer is very close to the surface in polar regions and at depths of several dm or 1 meter in equatorial latitudes [7].

3. When water vapour from Ceres is detected, the production rate is typically a few times 10^{26} s^{-1} [2,3,4].

4. The expansion velocity of the water vapour is ~400-700 m/s and the thermal velocity ~700 m/s, although a larger velocity > 1 km/s was observed on one occasion [3].

5. The water vapour does not originate from polar regions and is emitted from localized sources [3].

6. The occurrence of a transient exosphere observed by DAWN is correlated with solar proton events [4].

3. Possible mechanisms for water vapour release from Ceres

Here we review the mechanisms that were suggested for water vapour release from Ceres and evaluate them based on the observational results from the previous section:

A) Water from the interior of Ceres

As water ice is expected in the interior of Ceres, ice could sublimate far below the surface and diffuse through a porous subsurface layer [8]. However, the estimated production rate is ~2 orders of magnitude lower than the observed one, and as most of the water vapour is predicted to come from polar regions, it is not consistent with observations 5 and 6.

B) Cryovolcanism

Cryovolcanism is a process that may create water vapour with the observed properties (observations 3 and 4) and was suggested as an option [3]. However, no evidence for cryovolcanoes was found on Ceres by DAWN, and the process is inconsistent with observation 6.

C) Evaporation from recent large impact

A large recent impact could create temporary water activity by evaporation of the icy impactor and a newly created fresh crater. However, the process cannot explain the existence of more than one water source (observation 5) and the non-detection of a large crater with water ice at the surface.

D) Water ice sublimation

A straightforward way of creating water vapour is the mechanism of cometary activity: Sublimation of ice from either the surface or from just below it. While the mechanism is consistent with most observed properties of water vapour (observations 4-5), the observed amount of water ice is insufficient to explain the production rate. However, it is currently unknown how much water ice may be "hidden" from observations in an intimate ice-dust mixture on the surface, and impacts of small meteorites may locally remove the surface layer and thereby increase sublimation.
If sublimation is the dominant process, a separate explanation of observation (6) needs to be found.

E) Sputtering of ice by high energetic solar protons

This process, suggested by [4], is the only one that can explain observation 6. However, sputtering efficiencies appear too low to explain the observed production rates [9]. Also, the observed expansion velocities are on the low side for sputtered water. A more detailed investigation of the interaction of solar energetic particles with the surface and subsurface layer is needed to fully evaluate this process.

4. Conclusions

No known process can explain all observations. The most promising ones are (sub)surface sublimation and sputtering by high energetic protons, or a combination of both. We will present our detailed study of both processes to better evaluate what causes the water vapour leaving Ceres.

References

[1] McCord, T. B. and Sotin, C.: Ceres: evolution and current state. *J. Geophys. Res.*,Vol. **110**, E05009, 2005.

[2] A'Hearn, M. F., Feldman, P. D.: Water vaporization on Ceres. *Icarus*, Vol. **98**, pp. 54–60, 1992.

[3] Küppers, M. et al.: Localized sources of water vapour on the dwarf planet (1) Ceres. *Nature*, Vol. **505**, pp. 525-527, 2014.

[4] Villarreal, M. N. et al.: The Dependence of the Cerean Exosphere on Solar Energetic Particle Events. *Astrophys. J.*, Vol. **838**, pp. 8-12, 2017.

[5] Combe, J.-P. et al.: Detection of local H_2O exposed at the surface of Ceres. *Science*, Vol. **353**, aaf3010, 2016.

[6] Platz, T. et al.: Surface water-ice deposits in the northern shadowed regions of Ceres. *Nature Astronomy*, Vol. **1**, 0007, 2017.

[7] Prettyman, T. H. et al: Extensive water ice within Ceres' aqueously altered regolith: Evidence from nuclear spectroscopy. *Science*, Vol. **355**, pp. 55-59, 2017.

[8] Fanale, F. P., Salvail, J. R.: The Water Regime of Asteroid (1) Ceres. *Icarus*, Vol. **82**, pp. 97-110, 1989.

[9] Shi, M. et al: Sputtering of water ice surfaces and the production of extended neutral atmospheres. *J. Geophys. Res.*, Vol. **100,** No. E12, pp. 26387-26395, 1995.

EPSC Abstracts
Vol. 11, EPSC2017-287, 2017
European Planetary Science Congress 2017

Morphology of ring-mold craters within Occator crater

K. Krohn (1), R. Jaumann (1,2), K. A. Otto (1), K. Stephan (1), R. J. Wagner (1), F. Tosi (3), F. Zambon (3), I. von der Gathen (1), T. Roatsch (1), C. A. Raymond (4) and C. T. Russell (5)

(1) German Aerospace Center (DLR), Institute of Planetary Research, Berlin, Germany (katrin.krohn@dlr.de), (2) Freie Universität Berlin, Institute of Geological Sciences, Planetary Sciences and Remote Sensing, Germany, (3) INAF-IAPS, National Institute for Astrophysics, Rome, Italy, (4) Jet Propulsion Laboratory, California Institute of Technology, Pasadena, CA, USA, (5) UCLA, Institute of Geophysics and Planetary Physics, Los Angeles, CA, USA

Abstract

We found different shapes of ring-mold craters within in the huge ice-rich Occator crater on Ceres. The craters contain either a central pit or bowl or a central peak. The ice-rich material of Occator´s crater floor is supposed to have caused the formation of ring-mold craters.

1. Introduction

Ring-mold craters are common on lineated valley fill and lobate debris aprons on Mars. They are thought to be formed on layers with subsurface glacial ice [1]. Impacts into ice warm the ice and cause it to flow into the ring mold shape. We found similar craters within Occator crater on Ceres.

1.1 Data

For the analysis of craters Dawn Framing Camera (FC) data (monochrome and color ratio images) [2] from the Low Altitude Mapping Orbit (LAMO) with a spatial resolution of 35 m/px as well as a Digital Terrain Model (DTM) [3] derived from the High Altitude Mapping Orbit (HAMO) orbit data have enabled an initial characterization of the surface.

2. Observations

The observed craters are found within Occator crater and show an almost circular shape. The craters seem to be subsiding into the surface and, therefore, the rims are less elevated above the surrounding terrain. They show the typical ring-mold shape as known from Mars[1]. The craters contain either a central pit or bowl or a central peak (Fig. 1). The crater diameters range between 0.4 and 1.2 km.

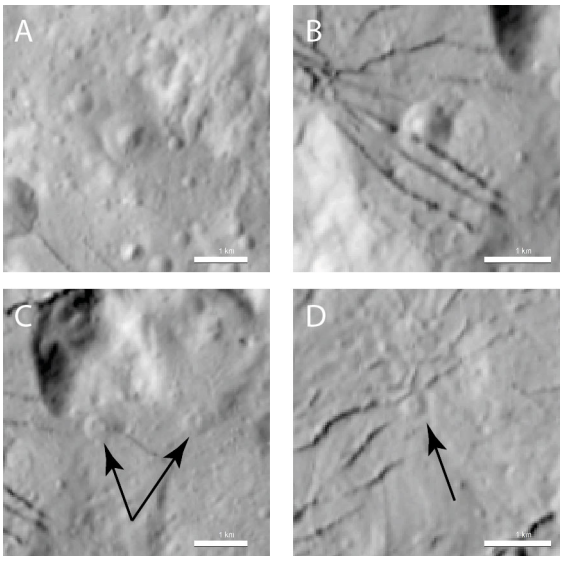

Figure 1: Ring-mold craters. A and B show craters with a central pit. C and D show craters with a central peak (arrows).

3. Summary and Conclusions

Latest results by the Dawn Spacecraft indicate that Ceres is a weakly differentiated body containing a shell dominated by an ice-rock mixture [4] and ammoniated phyllosilicates [5]. Recent observations

also show that hydrated salts could be warm enough to be mobile at a depth of 1.5-5 km below Ceres´ surface and would explain the buoyancy of ice and salt-enriched crustal reservoirs [6]. Occator is thought to be impacted in such a reservoir layer and triggered the mobility of ice and formed several ice-rich flow features and plain material [7]. The plains and flow materials also originate from the subsurface and their release is triggered by impacts [7].

So, it is likely that impacts hitting this material could form such ring-mold craters.

4. Future work

We will continue our survey of such craters all over Ceres and compare them to the Martian ones. The location of such craters provide important insight into detection of buried ice on Ceres.

Acknowledgements

We thank the Dawn team for the development, cruise, orbital insertion, and operations of the Dawn spacecraft at Ceres. Portions of this work were performed at the DLR Institute of Planetary Research, at the Jet Propulsion Laboratory (JPL) under contract with NASA, as well as the German Aerospace Center (DLR). Dawn data are archived with the NASA Planetary Data System. K. Krohn is supported by the Helmholtz Association (HGF) through the research Helmholtz Postdoc Program.

References

[1] Kress, A. M. and Head, J. W.: Ring-mold craters in lineated valley fill and lobate debris aprons on Mars: Evidence for subsurface glacial ice, GRL, Vol. 35, L23206, 2008.

[2] Sierks, H. et al.: The Dawn Framing Camera, Space Sci. Rev., 163, 263–327, 2011.

[3] Preusker, F. et al.; Dawn at Ceres - Shape model and rotational state, LPSC, March 2016, The Woodlands, Tx, USA, 2016.

[4] Fu et al.: The Global Scale Relaxation State of Ceres, AGU 2015, San Francisco, USA, 2015.

[5] De Sanctis M.C. et al.: Ammoniated phyllosilicates with a likely outer Solar System origin on (1) Ceres, Nature, 528, 241-244, 2015.

[6] Neumann W. et al.: Differentiation of Ceres and her present-day thermal state, LPSC, March 2016, The Woodlands, Tx, USA, 2016.

[7] Krohn et al.: Cryogenic flow features on Ceres: Implications for crater-related cryovolcanism, Geophysical Research Letters, 43, 1-10, 2016.

EPSC Abstracts
Vol. 11, EPSC2017-391, 2017
European Planetary Science Congress 2017

Conditions for Sublimating Water Ice to Supply Ceres' Exosphere

M.E. Landis (1), S. Byrne (1), N. Schörghofer (2,3), B.E. Schmidt (4), P.O. Hayne (5), J. Castillo-Rogez (5), M.V. Sykes (3), J.-P. Combe (6), A.I. Ermakov (5), T.H. Prettyman (3), C.A. Raymond (5), C.T. Russell (7)
(1) Lunar and Planetary Laboratory, University of Arizona, Tucson, AZ, USA (mlandis@lpl.arizona.edu), (2) Institute for Astronomy, University of Hawaii at Manoa, Honolulu, HI, USA (3) Planetary Science Institute, Tucson, AZ, USA (4) School of Earth and Atmospheric Sciences, Georgia Institute of Technology, Atlanta, GA, USA (5) Jet Propulsion Laboratory, California Institute of Technology, Pasadena, CA, USA (6) Bear Fight Institute, Winthrop, WA, USA, (7) Space Physics Center, Institute of Geophysics and Planetary Physics, Los Angeles, CA, USA

1. Introduction

OH^- and water vapor has been detected around Ceres [1,2], suggesting an exosphere. However, not all observations of Ceres have shown this exosphere [2], suggesting it is transient. One hypothesis to explain these detections is solar energetic particle events [3]. Another possible hypothesis is water ice sublimation. We model the conditions under which water ice sublimation can explain the transient detections of water vapor around Ceres. We conclude that surficial water ice exposures can produce the amount of vapor needed to match the observations of [2], if certain realistic constraints are met.

2. Model Description

We use a one-dimensional heat diffusion model in order to determine the temperatures in the near surface and surface. For water ice, we use an albedo of 0.135 [4], a heat capacity of 1615 J kg^{-1} K^{-1}, a thermal inertia of 2100 J m^{-2} K^{-1} $s^{-1/2}$, and a density of 925 kg m^{-3}. For regolith, we use an albedo of 0.09 [5], heat capacity of 837 J kg^{-1} K^{-1}, thermal inertia of 15 J m^{-2} K^{-1} $s^{-1/2}$ [6], and density of 1388 kg m^{-3}. We use a semi-implicit Crank-Nicholson scheme for stability and speed [e.g. 7].

We use a vapor production and diffusion model described by [8] in order to model global ice tables and locally exposed surface ice (Figure 1). For buried ice tables, we include the effects of a diffusive barrier to vapor release, composed of regolith grains with a porosity (ϕ) of 0.5 and a radius of 50 μm. We initially assume a depth to ice in this case of 3 cm, many diurnal skin depths such that $T_{depth}=\langle T_{annual}\rangle$. For exposed surface ice, we do not include the granular barrier to diffusion. We allow the volume fraction of regolith (C) to vary and assume the regolith content of the ice does not affect the ice thermal properties. Unless otherwise noted, we assume Ceres is a smooth oblate spheroid with an obliquity of 4°.

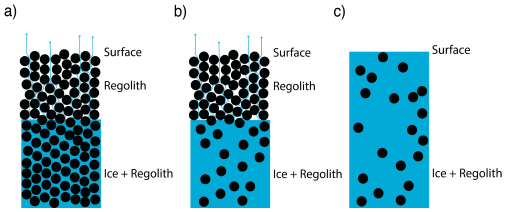

Figure 1: The different ice configurations explored in this paper: a) global buried pore-filling ice table, b) global buried pore-filling ice table, and c) exposed surface ice.

3. Sublimation from Buried Ice

We first examine the rate at which water vapor will be produced by buried ice (Figure 1a&b). As time increases, the amount of regolith that builds up on top of the ice increases and vapor escaping the surface decreases. We consider the C value of 0.5 (1-ϕ) for pore filling ice first. While pore-filling ice globally can produce close to the vapor production rate reported by [2] for a few million years, at 4.5 Gyr the vapor production falls several orders of magnitude short (Figure 2).

For excess ice, we consider $C<(1-\phi)$. We test two cases where: 1) the ice table can match the observed vapor output, and 2) the regolith build-up over 4.5 Gyr is consistent with the GRaND observations of hydrogen distribution [9] (Figure 2).

$C=7\times10^{-5}$ is sufficient for a global ice table to produce the observation of [2] but would result in an ice table detectable everywhere by GRaND, inconsistent with reported hydrogen depletion in the

upper 1m equatorward of 20°. C=0.02 would produce an ice table consistent with the GRaND results after 4.5 Gyr, but produces only about ~0.3 kg/s of water vapor (a factor of 10 too small). We cannot rule out some vapor production from a global ice table, but we can rule out a buried ice table (either excess or pore-filling ice) as a source of [2]'s observation.

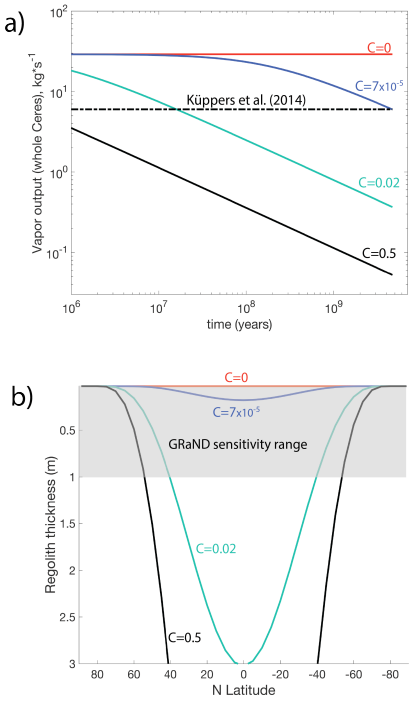

Figure 2: Results of vapor output (a) and regolith lag build up (b) with time for buried ice tables with varying regolith content.

4. Sublimation from Exposed Ice

If exposures of water ice (e.g. similar to the one reported in [4]) occurred close enough to the equator, the vapor produced over 1 km^2 is close to the vapor production rate of [2] (Figure 3). However, there are major seasonal and diurnal variations. Also, the effect of a crater similar to Oxo (latitude at 42.2° N, diameter 10 km, depth 1.5 km, parabolic shape) on the vapor flux is significant. This reduction is ~100 in the case of the approximate location of the Oxo exposed surface ice (maximum of ~0.5 kg s^{-1} km^{-2} on flat terrain to ~6 x10^{-3} kg s^{-1} km^{-2} on a poleward facing slope 3.3 km from the center of the crater).

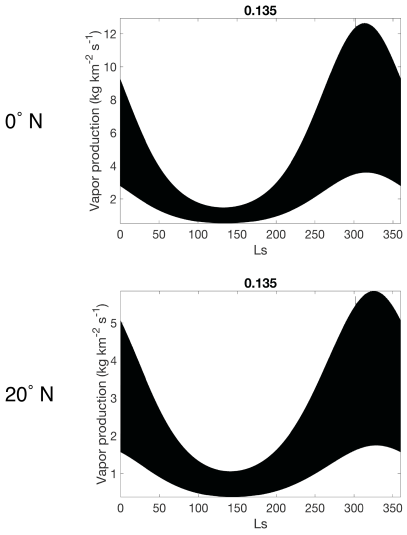

Figure 3: Vapor produced by exposed surface ice depending on latitude (labeled at left).

We calculate the amount of time it takes for a 100 µm (monolayer of regolith particles) lag to build up on these water ice exposures, reducing their albedo (0.135) to the background of Ceres (0.09). This is sensitive to the amount of regolith contamination assumed, but we find generally that water ice exposures close to the equator (the most likely to be able to produce the vapor reported by [2]) have lifetimes of less than ~3 terrestrial years. Therefore, if an ice exposure caused the vapor detection reported in [2], the ice would have faded to the background albedo by the time of the Dawn spacecraft's arrival.

References: [1] A'Hearn and Feldman, 1992. *Icarus* 98, 54 [2] Kuppers et al., 2014. *Nature* 505 [3] Villarreal et al., 2017, *AJL*, 838(1), doi: 10.3847/2041-8213/aa66cd/ [4] Combe et al., 2016. *Science* 353, aaf3010 [5] Li et al., 2016. *AJL*. doi: 10.3847/2041-8205/817/2/L22 [6] Rivkin et. al., 2011. *Space Sci. Reviews*, *163*(1), pp.95-116. [7] Parker, I. B., & Crank, J. (1964). *Computer Journal*, *7*(2), 163-167. doi: 10.1093/comjnl/7.2.163 [8] Schorghofer, 2008. *ApJ* 682, 697. [9] Prettyman et al. 2017. *Science,* aah6765

EPSC Abstracts
Vol. 11, EPSC2017-396, 2017
European Planetary Science Congress 2017

Landslides on Ceres Reveal Hidden Ice

B. E. Schmidt(1*), K. G. Hughson (2), H. T. Chilton(1), J. E. C. Scully(3), T. Platz(4), A. Nathues(4), H. Sizemore(5), M. T. Bland(6), S. Byrne(7), S. Marchi(8), D. P. O'Brien(5), N. Schorghofer(9), H. Hiesinger(10), R. Jaumann(11), J. Lawrence(1), D. Buczowski(5), J. C. Castillo-Rogez(3), M. V. Sykes(5), P. M. Schenk(12), M. C. DeSanctis(13), G. Mitri1(4), M. Formisano(13), J-Y Li(5), V. Reddy(5), L. LeCorre(5), C. T. Russell(2), C. A. Raymond(3) and the Dawn Science and Operations Teams. 1. Georgia Tech 2. UCLA 3. JPL 4. Max-Planck. 5.PSI. 6. USGS. 7. Univ. Arizona. 8. SWRI. 9. Univ. Hawaii. 10. Westfälische Wilhelms-Universität,. 11. DLR. 12. LPI. 13. INAF. 14. Universite de Nantes.

Abstract

We analyzed Dawn Framing Camera clear filter images of landslides on Ceres. Here we describe morphological evidence for an ice-rich substrate on Ceres based on both the geomorphology of landslide deposits and the characteristics of their failure scarps. Most of the results discussed here are reported in [1].

1. Introduction

Among the most compelling pre-Dawn questions about Ceres was in regards to the possibility of subsurface ice. Although unlikely on its surface, ice can last in Ceres' subsurface over billions of years if protected by an insulating layer; the necessary burial depth may be less than 1 m above ~40° latitude. We adopt the term "ground ice" to describe silicate material rich in ice, or silicate-covered ice deposits. The geomorphology of surface features can be related their material properties. In particular, landslides are found on planetary surfaces across the solar system, and are prevalent on ice rich bodies. On Ceres, these features have been observed associated with a surprising number of impact craters.

Across Ceres' surface there is evidence for mass wasting that operates in a very different manner from that on Vesta. Noted examples include scalloped and "breached" craters that are characterized by mass wasting by which recession of crater walls occurs in asymmetric patterns. Often contacts between craters are completely degraded, leaving behind lobate, or fan-shaped deposits.

2. Landslide Morphology

Arguably the most intriguing mass wasting features on Ceres manifest as flows with varying characteristics that originate at crater rims. In a survey of 20-35 km craters on Ceres (a good subset of features not strongly influenced by relaxation or secondary populations), a surprising number possess mass wasting features that extend 10's of km from their sources—over 20% contain such flows. The number of flows also varies with latitude, with a strong trend in the areal coverage of the surface by landslides that peaks above 60 degrees latitude. This poleward positive trend suggests that whatever is controlling the behavior of large mass wasting features on Ceres also varies with latitude. Thus, we consider ice as a likely culprit. Moreover, the style of mass wasting also changes over the surface of Ceres. We have identified three classes of flows that can be separated by their geomorphological characteristics. We refer to these as Type 1, 2, and 3

Type 1 flows are thick, tongue-shaped, lobate, and voluminous flows of up to hundreds of meters thick. Type 1 flows occur at a wide range of scales, from hundreds of meters to several kilometers long and tens to hundreds of meters thick. The always have one or more elongate trunks as wide as their source, often with longitudinal furrowing, with broad steep snouts and distal ramparts. Several high latitude craters feature long, thick flows that emanate from deep failures along degraded or slumping crater rims. In many of these cases, a small impact into the rim of a larger, older crater has destabilized material in and exterior to the crater rim. These flows may be consistent with downslope motion of relatively cohesive, ice-rich or ice-cemented material. Type 1 flows are only found above 50 degrees latitude.

Type 2 landslides are pervasive thinner (10's of m), spatulate, sheeted flows that initiate near crater rims at the exteriors of craters. The deposits of these features have circular to lobate toes, and from single broad or fan-shaped sheets to multiple sheets diverted by topography. Type 2 flows generally blanket low-

grade relief, but have impressive length despite their shallow slopes, characteristic of long run out landslides observed on other bodies such as Mars and Iapetus. The length and low slope angle of these flows suggests that friction reduction may help to explain these features, which requires ice but could also involve clays. Type 2 flows are found across the surface, though they are largely found above 30 degrees latitude, extending to 70 degrees. These are shallower features, perhaps restricted to forming within regolith.

Rare cases of cuspate, sheeted flows are observed extending outward from crater rims of extremely large impacts. In these features, thin broad sheets of smooth material terminate in layered sets of lobes or cusps. These flows are generally wider than the Type 2 flows and thinner than Type 1. Their acute lobes, absence of deep furrows, and textures--relatively smooth but occasionally hummocky—are similar to the morphology of fluidized ejecta blankets in Martian rampart craters and those on Ganymede that form by impacts into ice-rich ground. These flows may be consistent with melted material derived from the impact or post-impact melting. These are found in ~10% of craters below 50 degrees latitude and never at the poles.

3. Implications

Below, The geomorphology of Ceres' landslides is indicative of flow that occurs due to the presence of ice in the surface and shallow subsurface. These flow types are morphologically analogous to ice-rich flows found on Earth, Mars and the icy satellites. Importantly, no similar flow morphologies or fluidized materials were found on Vesta, which shares a comparable impact environment to Ceres. This indicates that the primary difference in impact response derives from target compositional differences. Material on Ceres appears weaker, more deformable, and flows more rapidly, than that on Vesta, which we interpret as evidence for ground ice. The increase in number of these flows towards the poles is evidence that Ceres' subsurface contains ground ice and that the ice is most abundant near the poles. Further, we characterize Type 1 and Type 2 as landslides, where Type 1 are relatively deeper failures, and Type 2 are shallower regolith-dominated features. Type 3 flows are most likely formed as either fluidized ejecta or by melting during the impaction.

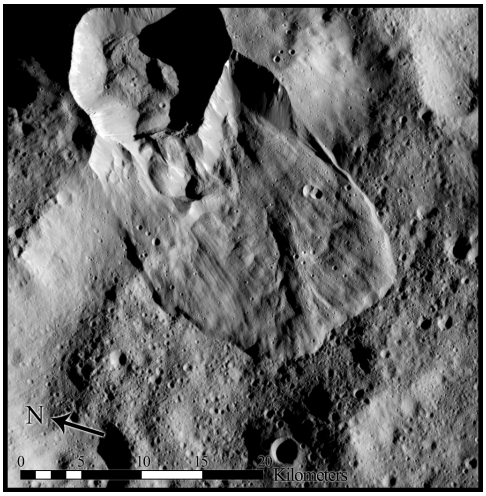

Figure 1: Type 1 landslide in Ghanan crater.

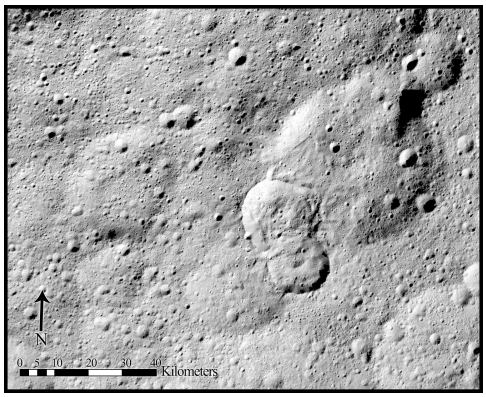

Figure 2: Type 2 landslide.

Acknowledgements

We acknowledge support from the Dawn mission, and the Framing Camera and mission operations team. Congratulations to Dawn on its 10th anniversary of launch!

References

[1] Schmidt, B. E. et al., (2017). Geomorphological evidence for ground ice on dwarf planet Ceres. Nature Geoscience 10, 383-343.

EPSC Abstracts
Vol. 11, EPSC2017-406, 2017
European Planetary Science Congress 2017

Dawn's Exploration of Vesta and Ceres

C. A. Raymond (1), C. T. Russell (2) and the Dawn Science Team.

[1]Jet Propulsion Laboratory, California Institute of Technology, 4800 Oak Grove Drive, Pasadena, CA 91001. Email: Carol.A.Raymond@jpl.nasa.gov, [2] Institute of Geophysics and Planetary Physics, University of California, Los Angeles, 595 Charles Young Drive East, Los Angeles, CA 90095. Email: ctrussell@igpp.ucla.edu.

Abstract

Dawn has revealed Vesta and Ceres to be unique, diverse fossils from the earliest epoch of our solar system. Vesta appears to be a surviving archetype of a differentiated, volatile-poor protoplanet, while Ceres is rich in volatiles. Ceres, the only dwarf planet in the inner solar system, bears affinity to outer solar system bodies.

1. Introduction

The Dawn mission launched in 2007 on a history-making ion-propelled journey to visit the two most massive bodies in the main asteroid belt and learn about the conditions and processes that shaped the early solar system. Dawn entered orbit around Vesta in July 2011 and explored the protoplanet for 14 months using its framing camera (FC), visible-infrared spectrometer (0.4-5μm; VIR), gamma-ray and neutron detector (GRaND) and by mapping the topography and gravity. Dawn recently completed its comprehensive mapping of Ceres and has since completed an extended mission. The main results and implications of the investigations of these two bodies, shown in Figure 1, are described below.

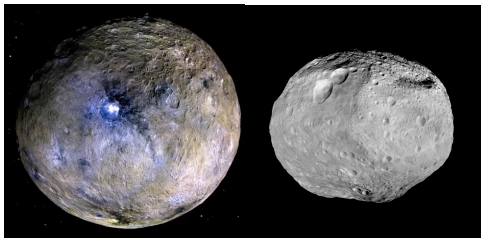

Figure 1: Left: A false color rendering of Ceres (~940-km avg diameter), draped on topography; Right: A gray-scale mosaic of Vesta (~530-km avg diameter) draped on topography.

2. Dawn at Vesta

Prior to Dawn's arrival, much had been inferred about Vesta's evolution from study of the HED meteorites, for which Vesta was the presumed parent. Dawn confirmed the Vesta-HED connection via surface lithologic mapping using VIR spectra [1, 2] and elemental chemistry from GRaND [3, 4], that showed most of the vestan surface is composed of howardite-like material with localized enrichments of eucrite and diogenite (Figure 2). A 110-km iron core was inferred from gravity and shape data, consistent with HED predictions [5]. While Vesta was found to be differentiated, as predicted by the HED paradigm, it appears to have experienced a complex magmatic history that resulted in lithologic diversity [e.g., 6]. Unexpectedly, broad, dark regions shown to be hydrogen-rich by GRaND [3] that also exhibit an OH absorption feature at 2.8 μm in VIR spectra [7], are interpreted to result from a few % of exogenic CM carbonaceous chondrite mixed into the regolith [8, 9]. Dawn also found pitted terrains [10] in young craters interpreted to be the result of outgassing of volatile-rich material, and gullies [11] thought to result from transient flow of water, both associated with impact processes. The discovery of hydrated material on Vesta's surface implies that delivery of volatiles to the inner solar system by primitive asteroids was an important process.

3. Dawn at Ceres

Prior to Dawn's arrival, Ceres was already known to be a dark, wet dwarf planet with evidence for altered minerals and water vapor emissions, from decades of ground- and space-based observations, and was thought to be at least partially differentiated. Dawn arrived at Ceres in March 2015 and found a heavily-cratered very dark surface that was punctuated by isolated, extremely bright areas [12]. This contradicted pre-Dawn model predictions of an ice-rich, viscously-relaxed smooth surface. Ceres is

shown to have a mechanically strong crust and is gravitationally relaxed at long wavelengths, implying that the strong crust overlies a weaker interior [13, 14]. Compositionally, Ceres' surface is dominated by dark material, ammoniated Mg-phyllosilicates, and carbonates [15-17]. The ubiquitous presence of ammoniated material (Figure 3) suggests formation in a colder environment, possibly in the outer solar system, while the overall mineralogy indicates Ceres' interior experienced pervasive alteration. Water ice has been observed in fresh craters at high latitudes, and elemental measurements indicate a shallow ice table [18]. These observations, along with Ceres gravity field [19] confirm that Ceres at least partially differentiated, providing evidence for an ancient subsurface ocean that may persist to the present. Local morphology such as crater floor deposits, isolated mountains and the enigmatic bright areas indicate active processes on Ceres that likely involve brine-driven cryovolcanism [20].

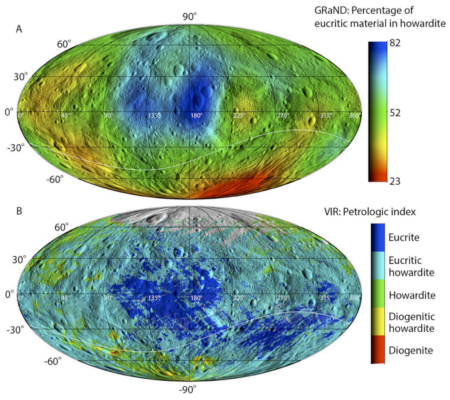

Figure 2. The distribution of Howardite, Eucrite and Diogenite on Vesta, as mapped by GRaND (top) and VIR (bottom).

4. Summary and Conclusions

Vesta is the parent body of the HEDs. It formed early from volatile-poor material with live Al^{26} and underwent a complex magmatic and geologic evolution. Ceres likely formed contemporaneously from volatile-rich material, partially differentiated, and underwent extensive aqueous alteration that moderated internal temperature. Ceres appears to have geologic activity at present. Radial mixing in the protoplanetary disk is evidenced in the history of these two sibling protoplanets.

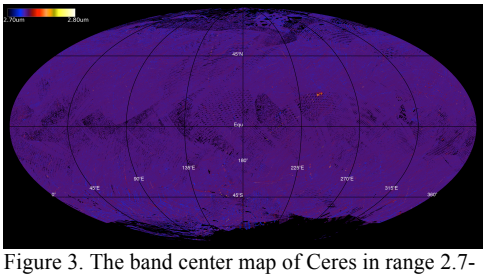

Figure 3. The band center map of Ceres in range 2.7-2.8 microns shows the nearly ubiquitous presence of ammoniated phyllosilicates across the surface [17].

Acknowledgements

Part of this research was carried out at the Jet Propulsion Laboratory, California Institute of Technology, under contract to the National Aeronautics and Space Administration.

References

[1] De Sanctis M. C. *et al.* (2012), *MAPS, 48*. [2] Ammannito E. *et al.* (2013), *MAPS, 48*. [3] Prettyman T. H. *et al.* (2012), *Science, 338*. [4] De Sanctis M. C. *et al.* (2012), *ApJ, 758*. [5] Raymond, C. A. *et al.* (2017), *Planetesimals*. Russell, C. T. *et al.* (2012), *Science*, *336*. [7] Prettyman T. H. *et al.* (2013), *MAPS, 48*. [8] McCord T. B. *et al.* (2012), *Nature, 291*. [9] Reddy V. e*t al.* (2012), *Icarus, 221*. [10] Denevi B. W. *et al.* (2012), *Science, 338*. [11] Scully J.E.C. *et al.* (2015), *EPSL, 411*. [12] Russell C. T. *et al.* (2016), *Science, 353*. [13] Bland M. T. *et al.* (2016), *Nat Geo, 9*. [14] Fu, R. R. *et al.* (2017), *EPSL, in press*. [15] De Sanctis, M.C. e*t al.* (2015), *Nature*, *528*. [16] De Sanctis, M.C. e*t al.* (2015), *Nature*, *536*. [17] Ammannito *et al.* (2016), *Science, 353*. [18] Prettyman T. H. *et al.* (2016), *Science, doi:10.1126/science.aah6765*. [19] Park R. S. *et al.* (2016), *Nature, 537*. [20] Ruesch, O. *et al.* (2016), *Nature, 353.*

EPSC Abstracts
Vol. 11, EPSC2017-507, 2017
European Planetary Science Congress 2017

TOPOGRAPHY AND GEOMORPHOLOGY OF THE INTERIOR OF OCCATOR CRATER ON CERES

R. Jaumann (1,2), F. Preusker (1), K. Krohn (1), I. von der Gathen (1), K. Stephan (1), K.-D. Matz (1), S. Elgner (1), K. Otto (1), N. Schmedemann (2), A. Neesemann (2), T. Roatsch (1,) E. Kersten (1), S. Schroeder (1), F. Schulzeck (1), F. Tosi (3), M.C. De Sanctis (3), D. Buczkowski (4), J.E.C. Scully (5), H. Hiesinger (6), C. Raymond (5), C. T. Russell (7), N.T. Stein (8), D.A. Williams (9), O. Ruesch (10), P. Schenk (11)
(1) DLR, Institute of Planetary Research, Berlin, Germany; (2) Freie Universität Berlin, Germany; (3) Istituto di Astrofisicae Planetologia Spaziali, INAF, Roma, Italy; (4) Johns Hopkins University Applied Physics Laboratory, Laurel, MD, USA; (5) Jet Propulsion Laboratory, California Institute of Technology, Pasadena, CA, USA; (6) Westfälische Wilhelms-Universität Münster, Germany; (7) UCLA, Institute of Geophysics, Los Angeles, CA, USA; (8) California Institute of Technology, Pasadena, Ca, USA, (9) Arizona State University, Tempe, TX, USA; (10) NASA Goddard, Greenbelt, MD, USA; (11) Lunar and Planetary Institute, Houston, Texas, USA.

Introduction: The potential presence of ice within Ceres' crust [1] raises the prospect of geological processes similar to differentiated icy bodies [2]. Dawn's spectral observations suggest some aqueous alteration, including the formation of clay materials [3,4], and possibly salts incorporated into a regolith layer characterized by small-scale compositional variations [5]. Thermal models suggest that Ceres is at least partially differentiated and could have undergone tectonic and cryovolcanic processes [1]. With a diameter of 92 km, Occator is one of the most prominent impact craters on Ceres. Its depth ranges from 4.8 km along the crater rim to -1.1 km at the crater floor with respect to a geodetic reference ellipsoid. Occator shows a set of specific features such as post impact formation crater filling, including multiple flow features, a central pit with a dome in its center, extensional tectonics expressed as linear radial and concentric graben, and spectral variations indicating a complex formation process.

Low Altitude Orbit Stereo Observation: We processed 550 LAMO stereo images from Cycle01 - Cycle11 with a resolution of ~ 35 m/pixel to generate a high-resolution digital terrain model (DTM) of the Occator impact structure. The image scale is 256 pixel per degree (~32. m/pixel) grid space. 1.8 billion surface points (~15 points per DTM grid) yield a calculated mean intersection error of +/- 2.8 m resulting in ~1.5 m height accuracy.

Materials in Occator: Occator shows a significant color variation between crater walls that havea reddish spectral slope, crater interior with a bluish spectral slope, and a whitish central part (Fig. 1) [5,6,7,8]. In general, blue to red color differences on Ceres are related with age [9] with blue units being younger than red ones and white material seems to be youngest. The white material of the dome and a deposit E of the center is composed of salts, mostly carbonates [5]. The bluish and reddish material seems to be composed of the same ammoniated phyllosilicates [3,4] but indicate a change in physical

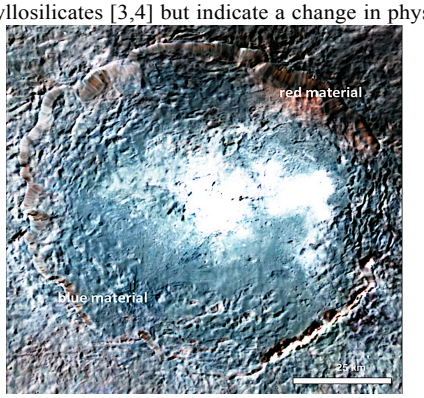

Fig. 1. Spectral contrast in Occator. Reddish crater wall material and bluish inner-crater plain material.

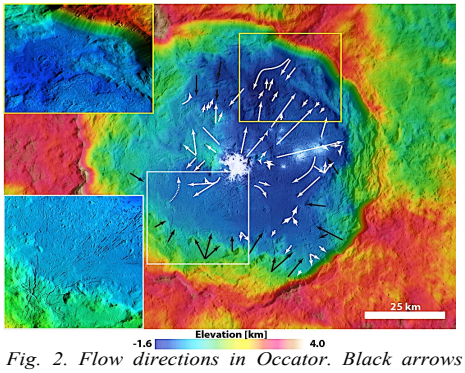

Fig. 2. Flow directions in Occator. Black arrows indicate mass wasting from walls and white arrows indicate bluish plains material originating from the center. Inlets: Flow features in the NE inner-crater plains. Tectonic extension features in the SW.

properties, mostly particle size [7,8].

Occator crater has mass wasting deposits origi-nating from the crater rims and walls and extending into the crater for 10 to 20 km. However, in the SE and NE these mass wasting deposits are completely covered by crater floor plains material that extends from the crater center to the rim, ponding against the crater walls (Fig. 2). The flows also superimpose the mass wasting deposits from the rims [9]. Furthermore, crater densities on Occator's interior deposits are slightly lower than on its ejecta blanket, indicating post-impact formation or target parameter variation between consolidated melt and unconsolidated ejecta deposits [6,10,11]. The terrain NW of the central area is very rough, shows mass wasting deposits, and is about 2 km thick w.r.t the rim of the central pit. The plains to the SE are smooth, pond against the crater wall, and are less than 500 m thick w.r.t. the rim of the central pit (Fig. 3). Assuming that the plains material superimpose the rim mass wasting in this area, the mass wasting deposits should be thinner in this part of the crater or the crater floor is tilted as possibly indicated by a 2 km lower crater rim in the SE. The central pit is about 3.5 km wide and 600 m deep while the dome rises 250 m within the pit [12]. In the NE, multiple flows approach the crater rim very closely. These flow plains are also less than 500 m thick w.r.t. the rim of the central pit. Some of the flows seem to have been superposed on the lower parts of the crater wall and then flowed back into depressions of the plain (Fig. 2). The flows to the NE appear to originate from the central region and move slightly uphill. This indicates either a feeding zone that pushes the flows forward by supplying low-viscosity material or an extended subsidence of the crater center, possibly after discharging a subsurface reservoir [6,9], or lateral oscillations of an impact melt sheet during emplacement. The SW crater area is also characterized by plain material ponding against rim wasting deposits with a complex and radially extending tectonic graben system about 50-100 m deep that reaches out to the central pit (Fig. 2). The plain material covers an area of about 4750 km^2 with an average depth of about 250 m resulting in a body of plains material of about 1200 km^3.

Conclusion: Mass wasting deposits resulting from the impact crater modification phase are mostly exposed in the W part while extended plains material about 500 m thick fills the crater interior from SW to NE superimposing the rim wasting deposits in these areas. Both materials are different w.r.t. their topography, geomorphology, and spectral characteristics, indicating a different genesis. The plains material seems to originate from the bright central pit/dome area and also exhibits extensional tectonic features and bright material deposits, indicating post impact processes in the plains material. In addition, the plains material is slightly younger than the impact event and the bright deposits are even younger than the plains material. Subsidence of the crater floor, the central depression, flows on the crater floor, the orientation and age of tectonics indicating post impact processes such as emplacement of flow materials, evaporation and hydrothermal processes which might be due to a long lasting impact melt pool or contact to subsurface cryo-magma.

Fig. 3. Cross sections through Occator crater

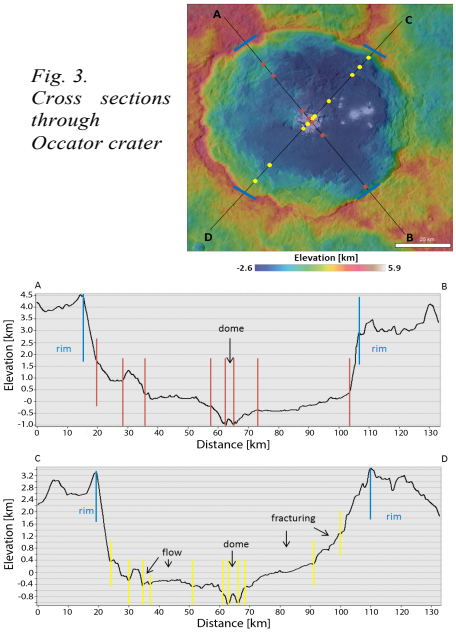

References: [1] J.B. Combe, et al., Science 353,1007 (2016). [2] C.T. Russell, et al., , Science 353, 1008 (2016). [3] M.C. De Sanctis, et al., Nature. 528, 241 (2015). [4] E. Ammannito, et al., Science 353, 1006, (2016). [5] M.C. De Sanctis et al., Nature, 536, 54. [6] R. Jaumann et al., LPSC, 47, 1455 (2016). [7] K. Stephan et al., GRL, in press (2017). [8] S. Schroeder et al., ICARUS, in press (2017). [9] K. Krohn et al, GRL, 43, 11994, (2016). [10] N. Schmedemann et al, GRL, 43, 11987. (2016) [11] A. Neesemann, et al., Icarus, in prep. [12] P. Schenk, et al., LPSC, 47 (2016).

EPSC Abstracts
Vol. 11, EPSC2017-553, 2017
European Planetary Science Congress 2017

Characterization of basaltic material in the outer Solar System.

S. Ieva (1), E. Dotto (1), D. Lazzaro (2), D. Fulvio (3), D. Perna (1,4), E. Mazzotta Epifani (1), M. Fulchignoni (4)
(1) INAF – Osservatorio Astronomico di Roma, Via Frascati 33, 00078 Monte Porzio Catone (Roma), Italy (simone.ieva@oa-roma.inaf.it) (2) Observatório Nacional, R. Gal. José Cristino 77, 20921-400 Rio de Janeiro, Brazil (3) Departamento de Física, Pontifícia Universidade Católica do Rio de Janeiro, Rua Marquês de São Vicente 225, 22451-900 Rio de Janeiro, RJ, Brazil (4) LESIA, Observatoire de Paris, PSL Research University, CNRS, Univ. Paris Diderot, Sorbonne Paris Cité, UPMC Univ., Paris 06, Sorbonne Université, 5 Place J. Janssen, Meudon Cedex F-92195, France

Abstract

The majority of basaltic objects in the main belt are dynamically connected to Vesta, the largest differentiated asteroid known. Others, due to their current orbital parameters, cannot be easily linked to Vesta and could be fragments of another differentiated asteroid. A recent statistical analysis performed by our group pointed out that, while basaltic objects in the inner main belt can be compatible with a Vesta origin, this seems not the case for basaltic asteroids beyond 2.5 a.u.
We present a spectroscopic survey for 25 basaltic candidates in the middle and outer main belt obtained between 2015 and 2016 at TNG and ESO-NTT.

.

1. Introduction

In the last decades several main belt asteroids have been found having a basaltic surface composition, similar to those of Vesta and basaltic achondrite meteorites. The discovery of a large basin in the southern hemisphere of Vesta [8,12] seemed to confirm the idea that a collisional event might have ejected basaltic fragments into orbits dynamically linked to Vesta, creating a dynamical family (the so-called *vestoids*).
The identification in the inner main belt of basaltic objects not members of the Vesta family [1,3] raised questions about the existence of other basaltic parent bodies, altough some of these non-Vestoids objects could have escaped from the Vesta family through resonant and/or non-gravitational effects [10].
Furthermore, the discovery of small basaltic objects in the middle-outer main belt not dynamically linked to Vesta [7,9] led to the idea that Vesta could not be the parent body for all the basaltic material in the Solar System, since at the moment there seems to exist no plausible transport mechanism able to convey Vesta's fragments beyond the 3:1 resonance.
Laboratory study on meteorites found that at least five other differentiated asteroids (D > 150-300 km) have existed in the main belt [13]. The lack of other great V-type asteroids discovered seems to suggest that these basaltic parent bodies were battered to bits, or that space weathering altered their spectral features. Finally, a recent review [6] pointed out that, while inner main belt V-types show similarities with Vesta, middle-outer V-types (MOVs) present a different mineralogy respect to the other basaltic material [5].

2. Results

We will present new visible reflectance spectra for 25 V-type MOV candidates obtained between 2015 and 2016 at Telescopio Nazionale Galileo (TNG) and ESO – New Technology Telescope (NTT). The observed objects were selected from different databases of putative V-type asteroids [2,11] and the analysis of their spectral parameters will be put in the context of the recent statistical analysis performed by our group [6]. We will also assess the effects of space weathering on basaltic surfaces at different heliocentric distances using laboratory analogues [4] and spectra characterized in our sample.

Acknowledgements

Part of this work was supported by the NEOShield-2 project (European Commission's Horizon 2020 program, contract No. PROTEC-2-2014-640351).

References

[1] Alvarez-Candal, A., Duffard, R., Lazzaro, D., Michtchenko, T. A&A, 459, 969, 2006

[2] Carvano, J. M., Hasselmann, P. H., Lazzaro, D., Mothé-Diniz, T, A&A, 510, A43, 2010
[3] Florczak, M., Lazzaro, D. Mothé-Diniz, T., Angeli, C. A., Betzler, A. S. A&A, 134, 463, 1999
[4] Fulvio, D., Perna, D., Ieva, S. et al., MNRAS, 455, 584
[5] Hardersen, P. S., Gaffey, M. J., Abell, P. A., Icarus, 167, 170, 2004
[6] Ieva, S., Dotto, E., Lazzaro, D. et al., MNRAS, 455, 2871, 2016
[7] Lazzaro, D., Michtchenko, T., Carvano, J. M. et al. Science, 288, 2033, 2000
[8] Li, J-Y, McFadden, L., Thomas, P.C. et al. Icarus, 208, 238, 2010.
[9] Moskovitz, N. A., Lawrence, S. Jedicke, R. et al. ApJ, 682, 57, 2008.
[10] Nesvorný, D., Roig, F, Gladman, B. et al. Icarus, 193, 85, 2008
[11] Oszkiewicz, D. A., Kwiatkowski, T., Tomov, T. et al., A&A, 572, A29, 2014
[12] Russell, C. T., Raymond, C. A., Coradini, A. et al. Science, 336, 684, 2012
[13] Scott, E. R. D., Greenwood, R. C., Franchi, I. A., Sanders, I. S.Geochim. Cosmochim. Acta, 73, 5835, 2009

EPSC Abstracts
Vol. 11, EPSC2017-596, 2017
European Planetary Science Congress 2017

Geological Evolution and Composition of the Dantu Crater

J. Kallisch (1), A. Nathues (1), T. Platz (1), G. Thangjam (1), K. Mengel (2) and M. Hoffmann (1)
(1) Max Planck Institute for Solar System Research, Goettingen, Germany, (kallisch@mps.mpg.de), (2) Clausthal Technical University, Clausthal-Zellerfeld, Germany

Abstract

The Dantu crater, located in the Vendimia Planitia depression at the northern hemisphere (centered at 24.3° N / 138.2° E) of dwarf planet Ceres, was investigated regarding its geological surface features and spectral appearance. For this purpose data of the Framing Camera (FC) and the Visible and Infrared Spectrometer (VIR) onboard the Dawn spacecraft were utilized and processed. Geological mapping of Dantu crater and its vicinity was conducted and absolute surface model ages were derived by measurements of crater size-frequency distributions. Dantu shows several features that are unevenly distributed in its northern and southern part, like fractures, bright spots and spectral properties. In this research we focus on possible processes that finally led to the observed dichotomies of the Dantu crater.

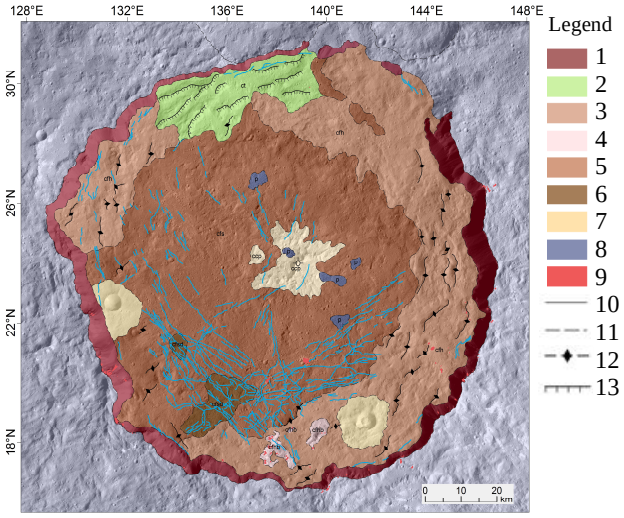

Figure 1: Geological mapping of the Dantu crater in stereographic projection. 1: crater wall, 2: crater terrace, 3: hummocky terrain, 4: bright hummocky terrain, 5: crater floor, 6: dark floor material, 7: central peak material, 8: pitted terrain, 9: bright spots, 10: accurate contact, 11: approximated contact, 12: ridge crest, 13 scarp.

1. Results

3.1 Geological context

With a diameter of ~120 km Dantu is well above the transition margin for a complex crater on Ceres and therefore shows remnants of a central peak and a wide, flat floor (Fig. 1). Our derived model age is 230 Ma +/- 30 by crater counting of the ejecta blankets. The north-eastern wall almost completely collapsed within an arc of ~40 km and only remnants are still visible. Terraces are only well preserved in the north-western segment of the crater rim. In other rim segments previously formed terraces are stronger eroded by ongoing mass wasting processes which led to an extensive formation of irregularly shaped hills, now referred to as hummocky terrain (Fig. 1). In most areas a sharp transition from the hummocky terrain to the much smoother crater floor exists. The crater density also lowers significantly when reaching the floor, indicating a younger surface age. No indications for melting events are found and thus we conclude that debris avalanches and granular flows filled up the central portion of the crater. The rectangular wall segments are further indications for crater wall collapse events that led to the formation of several avalanches. The most extensive and most recent one originated from a ~60 km wide wall segment of the south-west. In this area no hummocky terrain is found and the smooth floor material directly sets in at the bottom of the crater wall (Fig. 1). We see similarities at Occator, where the south-eastern part of the wall collapsed, resulting in a debris avalanche deposit that covers a large portion of the crater center [1]. Dantu shows a prominent system of fractures which are abundant in the southern portion but less frequent in the north (Fig. 1). Approximately 80 % of the southern fractures show a concentric orientation with respect to the crater center, spanning around half of the floor. Just a small number is radial orientated or shows no specific orientation. In some cases bright spots are associated with these fractures. We found more than 80 small bright spots with diameters between 100 and 500 m and a few with about 1 km diameter within the crater. Most of the bright spots are located in the southern crater wall and within a 10.5 x 9 km area in the southern hummocky terrain, showing a significantly higher albedo. The whole southern floor and hummocky

terrain area is on average about 1 km higher in elevation compared to the majority of the northern floor.

3.2 Mineralogical context

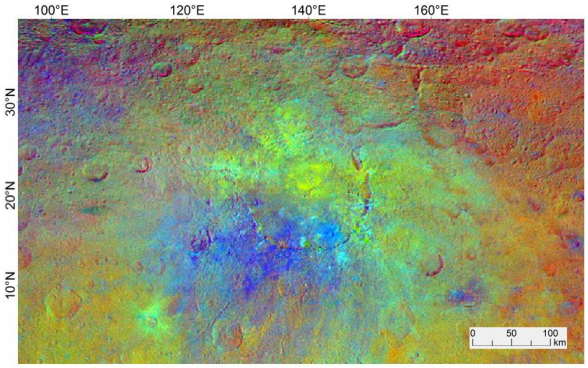

Figure 2: FC HAMO false color ratio mosaic in stereographic projection (R = 0.97/0.75 µm, G = 0.75 µm, B = 0.44/0.75 µm).

Comparison of the false color image with the geological map reveals a correlation between the bluish colors and floor and hummocky terrain in Dantu's south, which is also associated with a higher elevation and more abundant fractures and bright spots (Fig. 1, 2). Central and northern parts, however, show a more green-yellowish FC spectral slope. VIR IR spectra of the same areas do not show significant spectral variations. The typical Dantu spectrum exhibits, as the global average, strong absorptions around 2.7 µm, 3.1 µm and 3.9 µm, as well as some ambiguous absorptions around 3.2 – 3.5 µm and 4.2 µm. The 2.7 µm absorptions are associated with structural OH-groups in phyllosilicates [2]. The 3.1 µm absorptions are likely due to ammoniated phyllosilicates [3]. The 3.9 µm absorptions are consistent with carbonate phases [3, 4]. The spectra of the blue southern and the yellow-green central and northern areas don't show significant variations of the phyllosilicates and carbonates absorptions, which is an indication for similar mineralogy. This infers variations of physical parameters, such as grain size, to explain the differences in the FC color spectra.

2. Discussion

The measured elevation of 1 km of the southern portion of the crater and its higher abundance of fractures and bright spots is possibly caused by an ice/brine reservoir beneath the surface of Dantu's southern portion. The lower density of such a reservoir leads to uprising of the material and thus to extensional geological processes at the surface and eventually to the formation of fractures and bright spots. Alternatively the elevation could be explained by more extensive mass wasting of Dantu's southern terraces, indicated by a larger hummocky terrain area and the large debris avalanche which originated from the southwest. The concentric fracture system could then be explained by slowly inward slumping of the higher elevated area towards the north and the crater centre. A third possible scenario is an oblique impact from a northern direction. An impact angle of ~20° with respect to the surface normal could lead to the observed asymmetric crater floor profile without necessarily forming an elongated crater [5]. Furthermore, this scenario could provide a material sorting mechanism, leading to the observed spectral dichotomy and also explain the irregular distribution of the ejecta blanket.

3. Summary and Conclusions

Our study of Dantu revealed a diverse complex crater, showing non-uniformly distributed features like fracture systems, a high number of small bright spots, an asymmetric floor profile, uneven distributed spectral properties and an irregular ejecta distribution. The likeliest process that led to the observed dichotomies is a brine upwelling, causing extensional geological processes. However, large crater wall mass wasting and the possibility of an oblique impact, striking from the north, cannot be ruled out yet to be responsible for the heterogeneities.

References

[1] Nathues, A. et al.: Evolution of Occator Crater on (1) Ceres. The Astronomical Journal, Vol. 153, pp. 112–124, 2017.

[2] Lebofsky, L. A. et al.: The 1.7- to 4.2-µm spectrum of asteroid 1 Ceres: Evidence for structural water in clay minerals. Icarus, Vol. 48, pp. 453–459, 1981.

[3] De Sanctis, M. C. et al.: Ammoniated phyllosilicates with a likely outer Solar System origin on (1) Ceres. Nature, Vol. 528, pp. 241–244, 2015.

[4] Rivkin, A. S. et al.: The surface composition of Ceres: discovery of carbonates and iron-rich clays. Icarus, Vol. 185, pp. 563–567, 2006.

[5] Bottke, W. F. et al: Interpreting the Elliptical Populations on Mars, Venus and the Moon. Icarus Vol. 145, pp. 108–121, 2000.

EPSC Abstracts
Vol. 11, EPSC2017-637, 2017
European Planetary Science Congress 2017

Pitted terrains around Marcia crater on Vesta: strong eucritic absorptions and their implications

T. Giebner[1], K. Otto[1], R. Jaumann[1,2], S. E. Schröder[1], K. Krohn[1], K.-D. Matz[1], K. Stephan[1], F. Preusker[1], T. Roatsch[1].
(1) German Aerospace Center (DLR e.V.), Rutherfordstr. 2, 12489 Berlin, Germany, (2) Freie Universität Berlin, Malteserstr. 74-100, 12249 Berlin, Germany. (tanja.giebner@dlr.de)

Introduction

The NASA Dawn Mission orbited the asteroid Vesta in 2011/12 and obtained high resolution color images of its surface. The crater Marcia is roughly 60 km in diameter and the youngest large crater on the asteroid. In the broad surrounding of the crater, the Vestan regolith exhibits fairly diminished spectral characteristics with respect to Vesta's endogenic meteorite analogues, the HED's (howardite, eucrite, diogenite, e.g., [1], [2]). This is probably due to the input of spectrally darker material by impacts of different types of asteroids/meteorites (e.g., [3], [4]). Vesta also exhibits pitted terrains [5], most prominently present in and around the crater Marcia. In this study, we investigate an interesting spectral feature of some of the pitted terrains, which exhibit strong pyroxene absorption features consistent with those of eucrites, while their immediate surrounding does not show these prominent eucritic spectral characteristics (see Fig. 1).

Data and methods

We utilize Framing Camera color filters in order to identify the different spectral characteristics of Marcia crater and its surrounding with respect to the first pyroxene absorption band (i.e., the reflectance ratios 750/917, 965/830 and 965/917 [nm]). These data are then compared with different meteorite spectra (downloaded from the RELab database at Brown University, http://www.planetary.brown.edu/relabdocs/relab_disclaimer.htm) in order to infer the probable material composition. Additionally, we analyze high-resolution LAMO images (Low Altitude Mapping Orbit, ~ 20 m/px, [6]) and a digital terrain model [7] to reveal the geomorphological settings associated with the pitted terrains.

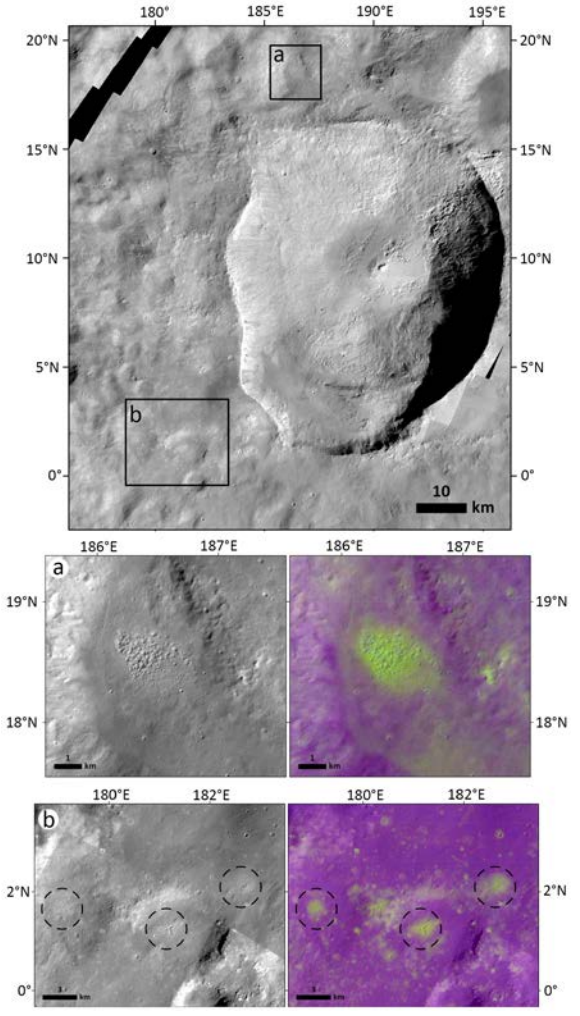

Figure 1: Pitted terrains around Marcia exhibiting spectral characteristics matching those of eucrites. a and b, left, display RGB images composed of R=F5/F4 (965/917 nm), G=F3/F4 (750/917 nm) and B=F5/F6 (965/830 nm), superposed on a LAMO clearfilter mosaic. Greenish/ yellowish colors correspond to stronger absorptions while purple/bluish colors correspond to diminished absorption features.

Spectral and Geomorphological Results

Marcia and its proximate surrounding show diverse spectral characteristics. The most eucritic (endogenic) spectral characteristics according to our spectral comparison with meteorites are locally confined and are found on the western crater rims, at the northwestern crater wall (around a young impact), at some of the pitted terrains located north and southwest of the crater and on some parts of the eastern crater rim. The color ratio data of the regolith material surrounding Marcia plot in an intermediate area between HED color ratio data and those of other meteorites like carbonaceous and ordinary chondrites for the analyzed color ratios.

The pitted terrain found on the floor of Marcia was reported to exhibit a lower reflectance than the average Vesta [5,8]. In contrast, we found that some of the pitted terrains in the immediate surrounding of Marcia, most of which occur within ~ 25 km of the current crater rim, exhibit strong pyroxene absorptions consistent with those of eucrites. The occurrence of those pitted terrains seems to be dependent on their location. The pitted terrain just north of Marcia and the pitted terrains found west/southwest of Marcia exhibit the most prominent eucritic characteristics, whereas the pitted terrains south/southeast of Marcia exhibit only very slight deviations of their spectral characteristics with respect to their immediate surrounding.

The digital terrain model [7] reveals that the pitted terrains do not always occur in topographic depressions. Instead, many of them are situated on a topographic slope.

Discussion

[5] have argued that the pitted terrains on Vesta likely formed by a similar process as on Mars, through volatile degassing. Previous studies have shown that in general, upon losing volatiles, spectra of natural materials become diminished and gradually lose their absorption features (e.g., [9]). This is not true for the pitted terrains surrounding Marcia which is intriguing.

The pitted terrains might be the result of a very young event, thus not exhibiting any space weathering effects described by [10]. However, the pitted terrains most likely formed during the impact process or shortly after. Otherwise, another process must be identified which could trap considerable amounts of volatiles long enough in the immediate subsurface of a regolith layer. Another explanation might involve the devolatilization process itself, which may have removed the darkening agents or darkening effects of other regolith constituents. The fact that some of the pitted terrains are located on topographic slopes might indicate uplift events after devolatilization occurred or different processes leading to those patterns that are not time dependent.

References

[1] De Sanctis, M. C., et al.: Spectroscopic Characterization of Mineralogy and Its DiversityAcross Vesta, Science, Vol. 336, pp. 697-700, 2012.

[2] Ammannito, E., et al.: Vestan lithologies mapped by the visual and infrared spectrometer on Dawn, Meteoritics & Planetary Science 48, Nr. 11, pp- 2185-2198, 2013.

[3] Jaumann, R., et al.: The geological nature of dark material on Vesta and implications for the subsurface structure, Icarus, Vol. 240, pp. 3-19, 2014.

[4] McCord, T. B., et al.: Dark material on Vesta from the infall of carbonaceous volatile-rich material, Nature, Vol. 491, pp. 83-86, 2012.

[5] Denevi, B., et al.: Pitted terrain on Vesta and implications for the presence of volatiles, Science, Vol. 338, pp. 246-249, 2012.

[6] Roatsch, T., et al.: High-resolution Vesta low altitude mapping orbit atlas derived from Dawn Framing Camera images, Planetary and Space Sciences, Vol. 85, pp. 293-298, 2013.

[7] Preusker, F., et al.: Global Shape of (4) Vesta from Dawn FC stereo images, Vesta in the Light of Dawn: First Exploration of a Protoplanet in the Asteroid Belt, LPI contribution No. 1773, p. 2027, Houston, Texas, 2014.

[8] De Sanctis, M. C., et al.: Mineralogy of Marcia, the youngest large crater of Vesta: Character and distribution of pyroxenes and hydrated material, Icarus, Vol. 248, pp. 392-406, 2015.

[9] Pommerol, A., et al.: The SCITEAS experiment: Optical characterizations of sublimating icy planetary analogues, Planetary and Space Sciences, Vol. 109-110, pp. 106-122, 2015.

[10] Pieters, C., et al.: Distinctive space weathering on Vesta from regolith mixing processes, Nature, Vol. 491, pp. 79-82, 2012.

EPSC Abstracts
Vol. 11, EPSC2017-643, 2017
European Planetary Science Congress 2017

Ceres surface temperatures: comparison between observation and theory

E. Rognini, M. T. Capria, F. Tosi, A. Frigeri, M. C. De Sanctis, E. Palomba, A. Longobardo, S. Fonte, M. Giardino, F. G. Carrozzo, A. Raponi, M. Ciarniello, E. Ammannito
INAF-IAPS, Rome, Italy

Abstract

Theoretical and observed temperatures on Ceres surface are compared. We calculate surface temperatures with a termophysical code that provides the temperature as a function of thermal conductivity and roughness. Preliminary results suggest low values for the thermal inertia.

1. Introduction

Thermal inertia is a fundamental parameter that controls surface temperature variations of airless body, and his value is sensitive to the presence of dust, regolith or rock; so this is an indicator of history and type of the surface material. Ceres and Vesta, the largest bodies in the main asteroid belt, are important to understand the early stages of solar system and the formation of terrestrial planets. The VIR instrument [1] onboard the NASA mission Dawn has allowed to measure the surface temperatures of these bodies, and a thermal analysis has been done for Vesta's surface, obtaining a map of its thermal inertia [2]. A similar kind of analysis is now being applied to Ceres.

2. The method

The VIR instrument is acquiring the spectra of Ceres in the range $0.25 - 5.1$ μm; the part of spectrum at $\lambda > 3.1$ μm is dominated by thermal emission so can be used to derive the temperatures (VIR is sensitive at temperatures above 180 K [3]). A termophysical model is used to compute theoretical temperatures. In order to obtain these temperatures we have to take into account the topography with the varying illumination angles. Ceres has an irregular shape, so a shape model is necessary. Surface temperature strongly depends on thermal conductivity. Different classes of thermal conductivity, corresponding to different kind of material (from lunar dust to regolith, in ascending order of thermal inertia) are considered. Ceres surface is divided into quadrangles and average temperatures are calculated iteratively by varying the values of roughness (a term characterizing topography at subpixel scale) and thermal conductivity class, until observed average temperatures are reproduced.

3. Summary and Conclusions

Preliminary analysis was made, restricted to a partial set of data that covers a limited portion of surface; this analysis suggest that Ceres' thermal inertia is low. We are now extending the analysis to the whole VIR data set: we are increasing surface under study, in order to obtain a thermal map as extended as possible.

Acknowledgements

VIR is funded by the Italian Space Agency and was developed under the leadership of INAF-Istituto di Astrofisica e Planetologia Spaziali, Rome, Italy. The instrument was built by Leonardo (Selex-Galileo), Florence, Italy. The authors acknowledge the support of the Dawn Science, Instrument, and Operations Teams. This work was supported by the Italian Space Agency and NASA. We thanks the Dawn Operation Team and the Dawn Science Team.

References

[1] M. C. De Sanctis et al., Space Sci. Rev., **163**, 329–360 (2011)

[2] M. T. Capria, F. Tosi, M. C. De Sanctis, F. Capaccioni et al., Geophysical Research Letters, **41**, 1438-1443 (2009)

[3] F. Tosi, M. T. Capria, M. C. De Sanctis et al., Icarus, **240**, 36-57 (2014)

EPSC Abstracts
Vol. 11, EPSC2017-691-3, 2017
European Planetary Science Congress 2017

Does Ceres have a transient exosphere? New HST observations.

L. Roth (1), N. Ivchenko (1), and N.J. Cunningham (2)
(1) KTH Royal Institute of Technology, Stockholm, Sweden
(2) Department of Physics and Astronomy, Nebraska Wesleyan University, Lincoln, NE, United States

Abstract

Ceres' exosphere appears to be very elusive. While some observations from Earth-based ground and orbiting telescopes indicate the presence of a water-based exosphere, other observations with similar sensitivity provided only upper-limits. A recent study suggests that a transient exosphere might be generated by solar energetic particle events. We report new observations of Ceres obtained with the Cosmic Origin Spectrograph (COS) of the Hubble Space Telescope (HST) in October 2016 in the search for exospheric emissions near Ceres. As for our previous COS observations of Ceres from 2015, we derive upper limits for oxygen abundances in the 2016 observations and investigate the solar wind conditions at the times of both the 2015 and 2016 observations.

1. Introduction

UV spectra taken by the International Ultraviolet Explorer revealed emission features from the OH A-X (0,0) band at 3085 Å near Ceres presumably resulting from dissociation of water vapor [1]. Global water vapor production rates of 10^{26} molecules/s were estimated from the measured OH brightness. Ground-based spectra with higher sensitivity taken in 2007 did not detect OH, constraining the production to $<7\times10^{25}$ molecules/s during the time of the observations [2]. Recently, water vapor was detected around Ceres by Herschel through absorption with a production rate of at least 10^{26} molecules/s [3], similar to the rate from the IUE detection.

1.1 Dawn mission

Shortly after the arrival of the Dawn mission at Ceres, bursts of energetic electrons were measured by the Gamma Ray and Neutron Detector (GRaND) and interpreted as signs for a bow shock [4]. These events are transient and might originate from a transient exosphere, which could be generated by a high flux of protons that was measured by GRaND before the electron bursts. Based on this finding, Villareal et al. [5] investigated the solar wind proton fluxes during the previous observations of Ceres' environment and found a positive correlation of high fluxes with exosphere detections.

2. HST observations 2015 & 2016

We observed Ceres at far ultraviolet (FUV) wavelengths using COS during two five-orbit visits by the Hubble Space Telescope on 26 August 2015 and on 26 October 2016. During the first visit in 2015, COS pointed at Ceres measuring sun light reflected off the surface as well as potential emissions from an exosphere. After subtraction of the surface-reflected light, no significant exospheric emissions were detected (Figure 1). The results from the first visit provided upper limits on the oxygen emission and were related to upper limit on an atomic oxygen column density of $(8.2 \pm 13.4) \times 10^{10}$ cm^{-2} [6]. Assuming that oxygen is produced by photodissociation of H_2O, we derive a conservative upper limit for the water production rate of 4×10^{26} molecules/s.

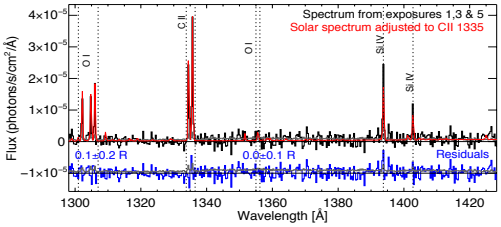

Figure 1: COS spectrum of Ceres UV emissions from 2015 providing upper limit on O abundance [6].

At the time of the first observations, the solar wind conditions indicate a very quiet period with low ion

fluxes through all energy channels of the ACE EPAM instrument (Figure 2). The non-detection of an exosphere during such quiet conditions is consistent with the presence of transient exosphere during high fluxes proposed by Villareal et al. [5].

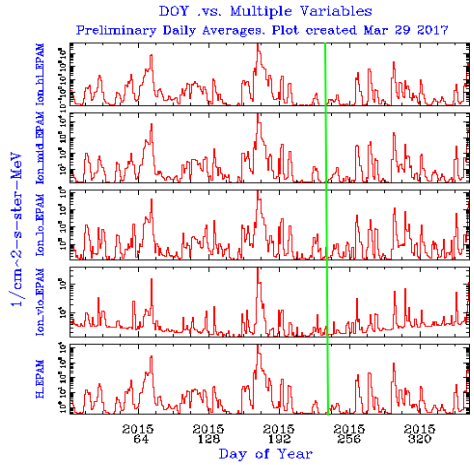

Figure 2: ACE EPAM solar wind ion and proton fluxes measured in 2015 around the HST/COS observation on 26 August (green vertical line).

During the 2016 visit, COS pointed to a region ~0.5 arcsec away from Ceres in order to search for exospheric emissions in absence of surface-reflected light. No significant emissions were measured in this region during the second HST visit either. We will compare the derived upper limits to the solar wind conditions for the 2016 observations and further investigate the consistency of our results with the theory of Villareal et al. [5].

3. Summary and Conclusions

We report HST/COS observations of Ceres taken on two occasions in 2015 and 2016, which provide independent constraints on the presence of an exosphere around the dwarf planet. No exospheric emissions were detected in the observations and upper limits on oxygen and water abundances are derived. The solar wind ion flux during the 2015 observations was particularly low and possibly insufficient for generating a detectable exosphere.

Acknowledgements

This work is based on observations made with the NASA/ESA Hubble Space Telescope, which is operated by the Association of Universities for Research in Astronomy, Inc., under NASA contract NAS 5-26555. These observations are associated with program 14106. L.R. appreciates the support from the Swedish VINNOVA agency and the Göran Gustafsson stiftelse.

References

[1] A'Hearn, M. F., and P. D. Feldman (1992), Water vaporization on Ceres, *Icarus*, *98*, 54–60, doi:10.1016/0019-1035(92)90206-M.

[2] Rousselot, P., E. Jehin, J. Manfroid, O. Mousis, C. Dumas, B. Carry, U. Marboeuf, and J.-M. Zucconi (2011), A search for water vaporization on Ceres, *Astron. J.*, *142*, 125, doi:10.1088/0004-6256/142/4/125.

[3] Küppers, M., et al. (2014a), Localized sources of water vapour on the dwarf planet (1) Ceres, *Nature*, *505*, 525–527, doi:10.1038/nature12918.

[4] Russell, C. T., et al. 2016, *Science*, 353, 1008

[5] Villarreal, M. N., et al. (2017). The Dependence of the Cerean Exosphere on Solar Energetic Particle Events. *The Astrophysical Journal Letters*, *838*(1), L8.

[6] Roth, L., Ivchenko, N., Retherford, K. D., Cunningham, N. J., Feldman, P. D., Saur, J., ... & Strobel, D. F. (2016). Constraints on an exosphere at Ceres from Hubble Space Telescope observations. Geophysical Research Letters, 43(6), 2465-2472.

EPSC Abstracts
Vol. 11, EPSC2017-758-2, 2017
European Planetary Science Congress 2017

Distribution of carbonates on Ceres

F.G. Carrozzo(1), M.C. De Sanctis(1), A. Raponi(1), E. Ammannito(2), J. Castillo-Rogez(3), B.L. Ehlmann(3,4), S. Marchi(1,5), N. Stein4, M. Ciarniello(1), F. Tosi(1), F. Capaccioni(1), M.T. Capria(1), S. Fonte(1), M. Formisano(1), A. Frigeri(1), M. Giardino(1), A. Longobardo(1), G. Magni(1), E. Palomba(1), F. Zambon(1), C.A. Raymond(3,4), C.T. Russell(6)

1. Istituto di Astrofisica e Planetologia Spaziali, INAF, Via del Fosso del Cavaliere 100, 00133 Roma, Italy; 2. Agenzia Spaziale Italiana, ASI, via del Politecnico, 00133 Roma, Italy; 3. Jet Propulsion Laboratory, California Institute of Technology, Pasadena, CA, USA; 4. Division of Geological and Planetary Sciences, California Institute of Technology, Pasadena, CA, USA; 5. Solar System Exploration Research Virtual Institute, SRI, 1050 Walnut Street, Boulder, CO 80302, USA; 6. Earth Planetary and Space Sciences, University of California, Los Angeles, CA, USA.

Abstract

In this work we mapped the spatial distribution of carbonates using the VIR/Dawn spectrometer. The presence of the hydrated carbonates indicates that their formation/exposure on Ceres' surface is geologically "recent" and dehydration to the anhydrous form (Na_2CO_3) is still ongoing.

Introduction

After the success of the Dawn mission in the study of the asteroid Vesta, the spacecraft departed toward the dwarf planet Ceres and is currently in its orbit. In this work we investigate the nature, the formation and the distribution of carbonates on Ceres using the VIR spectrometer onboard Dawn mission. Carbonates are a components of chondritic meteorites (e.g., 1,2) and have typically been used to infer the occurrence of liquid water in their parent bodies (3). The carbonate signature in the Ceres spectrum was first detected from Earth (4,5) and then confirmed by Dawn observations (6), showing that Ceres' average surface is an assemblage of phyllosilicates, ammoniated species, absorbing dark materials, and carbonates (6,7). The distribution and chemical composition of the carbonates are indicators of internal evolution.

Data

VIR (Visible-Infrared Mapping Spectrometer, 8) is the imaging spectrometer on board Dawn spacecraft and it is acquiring hyperspectral images in the 0.25-5.1 µm spectral range [1] of Ceres. We measured the strength and position of the ~3.9 µm feature across Ceres that gives us the distribution of carbonates unambiguously. The maps discussed have global longitudinal coverage, latitudinal coverage from 66°S to 66°N, and a spatial resolution of ~1.86 km/pixel at the equator. We used the HAMO dataset. A few selected small areas have been also observed at higher resolution, at ~100 m/pixel.

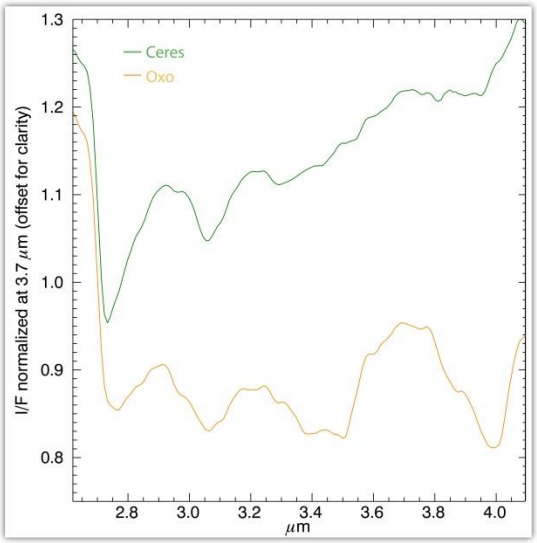

Fig. 1. Average spectrum of Ceres compared to the spectrum enriched in Na-carbonates located in Oxo crater. The spectra have been normalized to 1 at 3.7 µm and an offset has been applied for clarity.

Results

The VIR spectrometer mapped carbonates spatial distribution on the surface of Ceres. We found that carbonates are ubiquitous across the surface, but variations in the strength and position of their absorptions indicate variations in the composition and abundance of this mineral. The analysis of the band centers indicates that most of the surface is compatible with (Mg,Ca)-carbonates, being at about 3.96 µm. However, there are localized areas, such as

Occator central dome, that show band centers at much longer wavelengths (4.02 μm) typical of sodium carbonates (Fig. 1). Sodium carbonates occur mainly in the brighter areas of Ceres (9) and their geological settings suggest the upwelling, excavation and exposure of Na-rich species. The origin of sodium carbonate is different with respect the (Mg, Ca) carbonates, meaning that different processes have formed these chemical species.

Acknowledgements

We thank the Italian Space Agency (ASI), and NASA for supporting this work. The VIR instrument was funded and coordinated by the ASI and built by Selex ES, with the scientific leadership of the Institute for Space Astrophysics and Planetology, Italian National Institute for Astrophysics, Italy, and it is operated by the Institute for Space Astrophysics and Planetology, Rome, Italy. A portion of this work was carried out at the Jet Propulsion Laboratory, California Institute of Technology, USA, under contract to NASA. Dawn data are archived in NASA's Planetary Data System.

References

[1] B. Nagy, Geologiska Föreningen i Stockholm Förhandlingar, 88, 235-272 (1966).

[2] A. J. Brearley et al., 29th LPSC, abstract #1301 (1999).

[3] K. Fredriksson and F. Kerridge, Meteoritics & Planetary Science, 23(1), 35-44 (1988).

[4] A. S. Rivkin et al., Icarus, 185(2), 563-567 (2006).

[5] P. Beck et al., A&A, 526, A85 (2011).

[6] M. C. De Sanctis et al., Nature, 528, 241-244 (2015).

[7] E. Ammannito et al., Science, 353, 6303, (2016).

[8] M. C. De Sanctis et al., Space Science Review, 163, 329-369 (2011).

[9] N. Steins et al., Submitted, 2017

EPSC Abstracts
Vol. 11, EPSC2017-766-1, 2017
European Planetary Science Congress 2017

Photometric properties of Occator's bright spots analogue materials

M. Ciarniello, S. De Angelis, C. Carli and M. C. De Sanctis
INAF-IAPS, Rome, Itay (mauro.ciarniello@iaps.inaf.it)

Abstract

We report about the photometric properties at visible wavelengths of powders of Occator's bright spots analogue materials, as inferred from laboratory measurements.

1. Introduction

The VIR (Visible and Infrared Spectrometer) experiment [1] onboard the Dawn mission [2] extensively observed the surface of the dwarf planet Ceres in the 0.2-5.1 μm wavelength range. The surface of Ceres is characterized by a low albedo (geometric albedo 0.094±0.007 [3]) and spectral modeling of VIR observations indicates that the global composition is dominated by serpentine, NH_4-phyllosilicates and carbonates mixed with dark materials [4]. Nonetheless, at small scale, albedo and compositional variability is observed in the form of "bright spots" [5], with a notable example represented by the Cerealia Facula in Occator crater, whose reflectance at standard geometry is 7-8 times larger than the surrounding terrains [6]. Spectral modeling of Occator's bright spots observations from VIR [6] indicates in these areas a large concentration of carbonates (up to 45–80 vol%) mixed with a dark material, phyllosilicates and minor amounts of ammonium-bearing species.

In order to complement the results from spectral modeling of remote sensing observations and to further characterize the physical properties of Occator's bright spots, laboratory measurements of the spectral and photometric properties in the VIS-NIR wavelength range of the identified end-members and their mixtures are needed. In this work, we focus on the photometric properties of these materials, as derived from spectrophotometric measurements performed with the spectro-goniometer in the SLAB facility, at IAPS-INAF, Rome.

2. Spectrogoniometer - setup

The reflectance spectra of powders were measured with a Fieldspec-Pro spectrophotometer mounted on a goniometer. The spectra were acquired between 0.35 and 2.50 μm, with 1 nm spectral sampling and 2-12 nm spectral resolution from the visible to the near IR. The source used was a QTH lamp. The illuminated spot was ca. 0.5 cm^2. The calibration of the spectrophotometer was performed with 99% Spectralon® optical standard (registered trademark of Labsphere, Inc.). The goniometer is PC-controlled and permit to vary incidence (inc) and emission (emi) angles in the principal scattering plane with phase angles (α) from 30° to 130°. The illumination and the detector instantaneous field of view cones are approximately 6° wide.

3. End-members and mixtures

The investigated materials are represented by: Natrite [Na_2CO_3], Ammonium Chloride [NH_4Cl], Illite [$K_{0.65}Al_2(Al_{0.65}Si_{3.35}O_{10}$ $(OH)_2$], Magnetite [Fe_3O_4] and an intimate mixture ("bright spot mixture") of these end-members (50.5 %wt Natrite + 2.5%wt + 14%wt Illite +33%wt Magnetite). All the end-members and the mixtures have been prepared for various grain sizes ranges: <36 μm, 36-50 μm, 50-75 μm, 100-150 μm and 150-800 μm.

4. Measurements

We plan to measure reflectance spectra of single end-members and mixtures at various observation geometries in the principal scattering plane with incidence and emission angles ranging in the 0°-65° interval and phase angles from 30° to 90°.

5. Preliminary results

In Fig. 1 the reflectance factor (REFF) at 0.7 μm for the single end-members and the "bright spot mixture" at grain size <36 μm is reported as a function of the

incidence and emission angles respectively. Natrite (nat1) and Ammonium Chloride (cla1) show the highest albedos of the samples while magnetite (mgt1) is characterized by a very low reflectance. The reflectance level of the "bright spot mixture" is ~0.2 at inc =30°, emi=0°, α=30° slightly lower than the value derived from VIR measurements at 0.55 μm (I/F=0.26 corresponding to REFF = 0.3). The REFF curves are not exactly symmetrical for inc-emi exchange, possibly due to residual systematics error in the measurements.

In Fig. 2 the REFF curves of the "bright spot mixture" and Illite (imt2) are shown as a function of the phase angle for specular observation geometries (inc = emi). It can be noticed that while the Illite sample exhibits an isotropic scattering behavior, the "bright spot mixture" appears relatively forward-scattering.

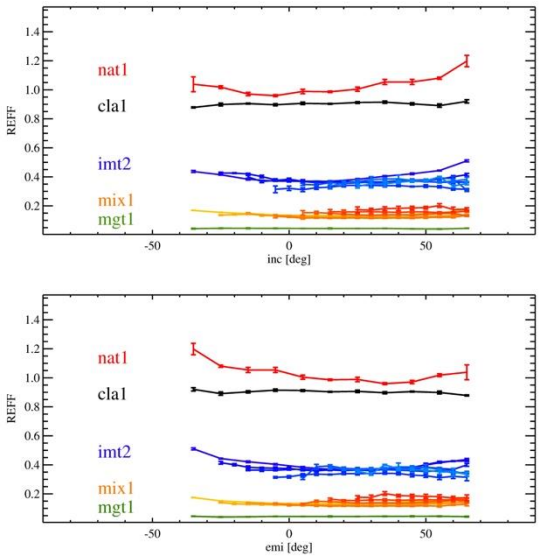

Figure 1. REFF curves at 0.7 μm as a function of incidence (top panel) and emission (bottom panel) angles for Natrite (nat1), Ammonium Cloride (cla1), Illite (imt2), Magnetite (mgt1) and bright spot mixture (mix1). The sign of the incidence and emission angles discriminate between opposite positions in the principal scattering plane with respect to the normal at the sample plane. Incidence and emission directions in the same semi-plane have opposite signs. Phase angle α=inc+emi is 30°. Different colored curves for imt2 and mix1 correspond to different phase angles (from 30° to 90°) (Figure 2).

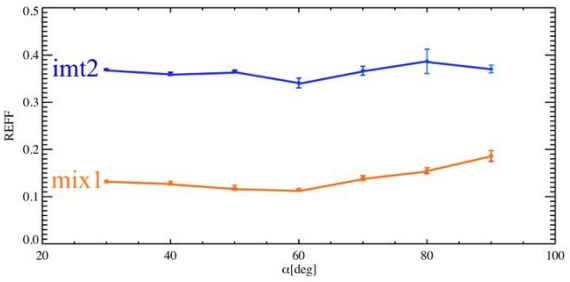

Figure 2. REFF curves at 0.7 μm as a function of phase angle (α) for Illite (imt2), and "bright spot mixture" (mix1) for specular observation geometries (inc=emi).

6. Summary

REFF curves for the materials and the observation geometries described in Sec. 3 will be measured, allowing us to characterize the photometric behavior of single end-members and mixtures. Along with this, the effect of the grain size on the photometric properties of the end-members and their mixtures will be investigated. Comparison of these measurements with the photometric properties of Occator's bright spots as derived from Dawn remote sensing instruments (VIR, FC) will provide further insights on the physical properties of the regolith.

Acknowledgements

This work is supported by an Italian Space Agency (ASI) grant.

References

[1] De Sanctis et al. 2011, Space Sci. Rev., 163, 329.

[2] Russell, C. T., & Raymond, C. A. 2011, Space Sci. Rev., 163, 3.

[3] Ciarniello et al., 2017, A&A, 598, A130.

[4] De Sanctis et al., 2015, Nature, 528, 241.

[5] Palomba et., 2017, Icarus, submitted.

[6] De Sanctis et al., 2016, Nature, 536, 54.

EPSC Abstracts
Vol. 11, EPSC2017-820-1, 2017
European Planetary Science Congress 2017

Dynamic models for formation of Occator bright spots

B. Travis (1), P. Bland (2), W. Feldman (1) and M. Sykes (1)
(1) Planetary Science Institute, Tucson, AZ, USA (btravis@psi.edu), (2) Curtin University, Perth, Australia

Abstract

A prominent feature of the asteroid Ceres is the large crater Occator, and especially the bright spots seen in its interior. We describe possible mechanisms that could have formed the bright spots and the central pit.

1. Introduction

The Occator crater has a diameter of 92 km and a depth of 4 km. It is located at latitude 19.86 ^{o}N. A central pit has a diameter of 11 km and depth of 0.6 km. The age of the crater is estimated at 16-280 Myrs [1,2], while the bright spots are apparently much younger, potentially present-day. The bright spots appear to be rich in carbonate deposits [3]. A previous study [4] has proposed that the bright spots in Occator are the result of outflow to the surface from a subsurface brine reservoir. Build-up of gases (CO_2 and CH_4) in the reservoir according to [4] lead to explosive breaching of the surface. Impact energy is likely to have stimulated near-surface hydrothermal circulation [5], but the time-scale of that process would occur much closer to the creation of Occator, rather than tens of Myrs or more later. Post-impact hydrothermal systems tend to last no more than ~1 Myrs [5]. The time difference suggests that a considerably deeper reservoir is being tapped.

Numerical simulations of the evolution of Ceres from an unconsolidated cold mixture of rock grains and ice crystals to the present indicate that throughout much of Ceres' history, hydrothermal circulation can occur in the core and in a muddy ocean mantle [6]. Heat generated by radiogenic elements and heat of reaction from serpentinization drive fluid circulation. The initial size distribution of rock grains includes coarse particles and fine particles. When the interior warms sufficiently to melt ice, rock grains are freed up; they settle at size-dependent rates towards the core.

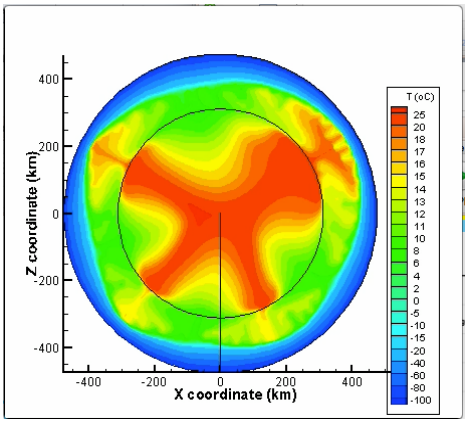

Figure 1: Snapshot of thermally driven convection showing multiple scales of circulation. The interior circle is the boundary of a porous Ceres core.

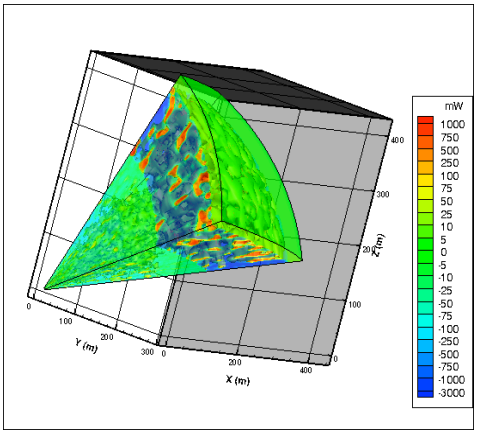

Figure 2: Higher resolution mud convection in a sector, showing clearly the many episodic plumes that rise toward the surface.

Resultant core size and core and mantle densities lie on the curve of possible solutions determined by gravity analysis [7], between CM and CI models. Fine particles (< 1 μm) remain suspended; the fluid is a mud. Despite the higher viscosity of mud compared to pure water, hydrothermal circulation is still possible. Figures 1 and 2 captures the very dynamic multi-scale circulation that could develop.

2. Tapping a deep reservoir

Several processes could transport brine from deep in Ceres to the surface or near surface, based on our model results [8]. (1) Flow through fractured mantle. Over time, the model mud mantle gradually freezes, but not uniformly in latitude or longitude, generating vertical and lateral stresses on the neighboring unfrozen upwellings. Compressibilities of water and rock are about 4.5×10^{-5} /bar. Applying that to the H_2O phase change (about 10% volume change x ~0.50 water volume fraction) generates about 1 kbar of overpressure, sufficient to fracture ice and rock and drive out-flow to the surface or near-surface, until excess volume is expelled. We envision a slow buildup of pressure and then a relatively sudden breakthrough when a critical pressure is reached and a fracture conduit is formed. Hydrothermal circulation is episodic meaning the process of freezing and fracturing would also be episodic. (2) As the mud layer freezes, cryo-convection (convection in the solid phase), will increase in strength (Figure 3). Occator crater is located at low latitude, just where convection, either hydrothermal or cryo, should be strongest. The base of a cryo-convective plume would lie at the top of a regional mud sea. Salts and other minerals in the sea mud would be entrained into the upwelling plume, and eventually brought to the near-surface. (3) Episodic porous flow through the overlying frozen mantle. Deep regional mud seas persist to the present time in our model. Further, experimental studies of slow freezing rates in particle rich solutions [9] indicate that a pattern of alternating layers of ice and particulates is likely to form, with vertical micro-fractures connecting the layers locally. The overlying frozen mantle could be somewhat permeable. An impact would also increase permeability through extensive fracturing. When the crater forms, there is a sudden pressure deficit of roughly 25 bars. This pressure difference could drive flow of brine on a **tens of** Myr time scale from a depth of ~100 km.

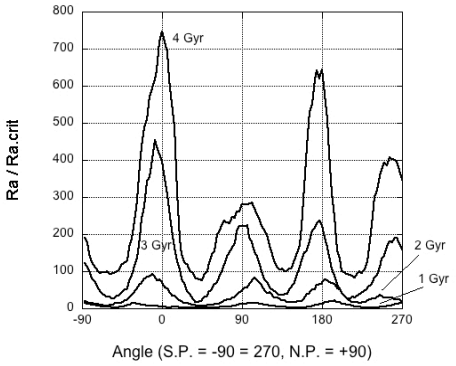

Figure 3: Possibility of cryo-volcanism increases over time as the mud mantle freezes. Further, the higher the Ra number, the more episodic the plume generation becomes.

In summary, there are several mechanisms, acting either separately or simultaneously, that could bring H_2O and minerals from deep in Ceres to a near-surface reservoir.

References

[1] Nathues, A., et al.: Plan. Sp. Sci., in press.
[2] Jaumann, R., et al.: Age-dependent morphological and compositional variations on Ceres, LPSC 47, #1455, 2016.
[3] De Sanctis, M.C., et al.: Bright carbonate deposits as evidence of aqueous alteration on (1) Ceres, Nature 536, 54, 2016.
[4] Nathues, A., et al.: Evolution of Occator crater on (1) Ceres, LPSC 48, # 1385, 2017.
[5] Barnhart, C., Nimmo, F., Travis, B., Martian post-impact hydrothermal systems incorporating freezing, Icarus 208, 101–117, 2010.
[6] Travis, B., Bland, P., Feldman, W., Sykes, M.: Unconsolidated Ceres model has a warm convecting rocky core and a convecting mud ocean, LPSC 46, # 2360, 2015.
[7] Park, R., et al.: A partially differentiated interior for (1) Ceres deduced from its gravity field and shape, Nature, doi:10.1038/nature18955, 2016.
[8] Travis, B., Feldman, W., Sykes, M.: Ceres model suggests large scale topography may reflect early time internal convection, LPSC 47, #2762, 2016.
[9] Anderson, A., & Worster, M.: Periodic ice banding in freezing colloidal dispersions, Langmuir, 28, 16512, 2012.

EPSC Abstracts
Vol. 11, EPSC2017-821, 2017
European Planetary Science Congress 2017

Water ice in Juling crater on Ceres surface: method for properties retrieval

A. Raponi[1], M.C. De Sanctis[1], M. Ciarniello[1], E. Ammannito[2,1], A. Frigeri[1], J.-Ph. Combe[3], F. Tosi[1], F. Zambon[1], F.G. Carrozzo[1], G. Magni[1], M.T. Capria[1], M. Formisano[1], A. Longobardo[1], E. Palomba[1], C.M. Pieters[4], C.T. Russell[5], C.A. Raymond[6], and the Dawn/VIR Team
[1]INAF-IAPS Istituto di Astrofisica e Planetologia Spaziali, Rome, Italy (andrea.raponi@iaps.inaf.it), [2]Agenzia Spaziale Italiana, Rome, Italy. [3]Bear Fight Institute, Winthrop, WA, USA. [4]Department of Earth, Environmental and Planetary Sciences, Brown University, Providence, RI, USA. [5]University of California at Los Angeles, Los Angeles, CA, USA. [6]NASA/Jet Propulsion Laboratory and California Institute of Technology, Pasadena, CA, USA.

Abstract

Spectral signatures diagnostic of water ice were detected in localized areas on the surface of Ceres usingthe Dawn/VIR instrument [1] of the Dawn spacecraft. The current study analyzed water ice detected in a shadowed region of Juling crater. Water ice properties were derived by a Hapke radiative transfer model [2].

1. Introduction

The NASA Dawn spacecraft in orbit around Ceres has been acquiring a huge amount of data at different spatial resolutions during the several phases of the mission that started in 2015. The Visible and InfraRed (VIR) mapping spectrometer [1] onboard Dawn, enabled detection and mapping of the main mineralogical phases on Ceres.
The surface of Ceres is mainly characterized by a large abundance of dark component, NH_4-phillosilicates and carbonates [3]. Other mineralogical phases, such as water ice, also exist at local scale [4, 5] . Water ice detected in Juling crater (lon=168°, lat=35°S) is not under direct solar illumination. However, it is visible becouse of secondary illumination coming from the crater floors and rims. A specific modeling is required to derive water ice properties such as abundance, grain size, phase, type of mixture with the average dark terrain of Ceres, and surface temperature.

2. Dataset

Water ice in Juling crater has been detected during the High-Altitude Mapping Orbit (HAMO) phase (resolution ~400 m/px) and the Low Altitude Mapping Orbit (LAMO) phase (resolution ~100 m/px). We take into account an area on the northern rim which include an ice rich wall (Fig. 2) large enough to be spatially resolved even at the lowest resolution and that includes all the pixels of water ice signatures.

3. Method

The region of interest is in shadow. However, its signal can be detected using the light reflected by the crater. The radiance coming from the illuminated outer region is affecting the total signal collected in the shadowed region because of the Point Spread Function of the instrument (Fig. 1): the signal of the outer illuminated region is scattered in the adjacent pixels.
To account for this effect we model the signal collected (Eq. 1) as a weighted average of the signal from outer region (OR) (Eq. 2) and signal of the shadowed region (SR) (Eq. 3). The weights of these two different terrains are then retrieved by a best fitting procedure.
Moreover, the regolith of the shadowed ice-rich region (Eq. 2) is modeled by an areal mixture of water ice (WI) (optical constants by [6, 7, 8]), and Ceres' average terrain (CAT) with optical properties as defined by [9].

Eq. 1) $Refl_{average} = [Rad_{SR} * p_{SR} + Rad_{OR} * p_{OR}] / J$
where:
$Refl_{average}$ = average reflectance;
P_{SR} = cross section of the ice-rich shadowed region as a fraction of the total projected area of interest;
$p_{OR} = (1 - p_{SR})$ = cross section of the outer regions as a fraction of the total projected area of interest.

Eq. 2) $Rad_{OR} = J * r_{R\_OR}$
where:
Rad_{OR} = radiance of the outer regions;
J = solar irradiance;
r_{R_OR} = bidirectional reflectance [2] of Ceres' average terrain, with photometric parameters as defined by Ciarniello et al. (2016), and viewing geometry by

shape model analysis and spacecraft attitude at the moment of the observations;

Eq. 3) $Rad_{SR} = J * (r_{s\_CAT} <\mu_0> / \pi) /2 * [r_{s\_WI}\, p_{WI} + r_{s\_CAT}\, (1- p_{WI})]$

where:

Rad_{SR} = radiance of the shadowed ice-rich region;

r_{s_CAT} = bihemispherical reflectance [2] of Ceres' average terrain, it is used instead of the bidirectional reflectance because the secondary illumination hitting the shadow comes from all direction within ~π steradians;

$<\mu_0>$ is the average incidence angle cosine on the crater at the time of the observation, derived by shape model analysis;

the term $(r_{s\_CAT} <\mu_0> / \pi)$ represents the reflectance of a Lambertian surface, with Lambert albedo equal to r_{s_CAT} [2]; the factor 2 at denominator accounts for the fact that one half of the whole solid angle seen by the ice-rich wall is covered by the crater itself; higher orders of scattering are assumed as negligible.

r_{s_WI} = bihemispherical reflectance [2] of water ice;

p_{WI} = cross section of water ice as a fraction of the total projected area of the ice-rich shadowed region.

We model $Refl_{average}$ (Eq. 1) using a least square optimization algorithm that fitted the measured reflectance (similarly to [10]) to retrieve an unambiguously estimate of p_{SR} and p_{WI}.

Acknowledgments

The Visible and InfraRed mapping spectrometer (VIR) was funded and coordinated by the Italian Space Agency and built by SELEX ES, with the scientific leadership of the Institute for Space Astrophysics and Planetology, Italian National Institute for Astrophysics, Italy, and is operated by the Institute for Space Astrophysics and Planetology, Rome, Italy.

References

[1] De Sanctis M.C. et al., SSR 163, 2011.
[2] Hapke B., Cambridge Univ. Press., 2012.
[3] De Sanctis M.C. et al., Nature 528, 2015.
[4] Combe J.-Ph. et al., Science 353, 2016.
[5] Combe J.-Ph. et al., DPS-EPSC, 2016.
[6] Mastrapa R. M. et al., Icarus, 2008
[7] Mastrapa R. M. et al. , Astrophysical Journal, 2009
[8] Clark R. N. et al., Icarus, 218, 831, 2012.
[9] Ciarniello M. et al., A&A 2017
[10] Raponi A. et al., 2016, MNRAS 462.

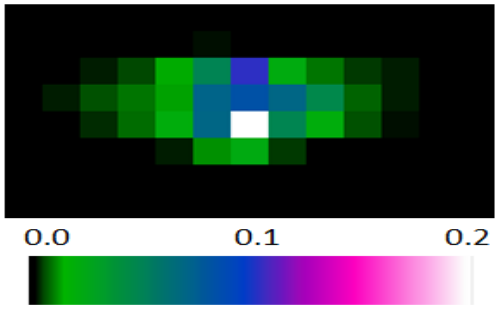

Figure 1. Point Sprad Function of VIR instrument as derived by a star observation.

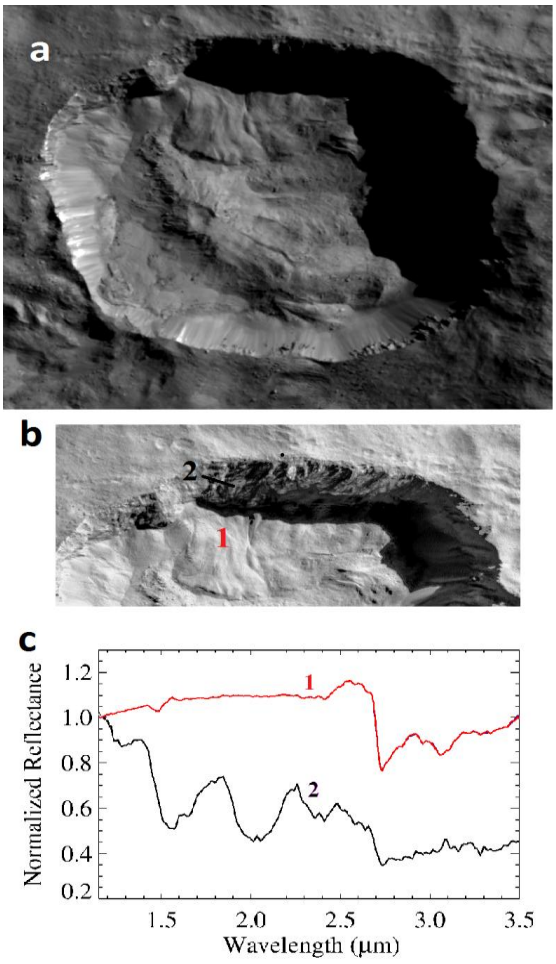

Figure2. Panel a) Juling crater: Framing camera mosaic. Panel b) Region of interest where shadows are enhanced in order to see the details. Panel c) typical spectra outside and inside the ice- rich shadowed.

EPSC Abstracts
Vol. 11, EPSC2017-837, 2017
European Planetary Science Congress 2017

Differentiation Models of Vesta and Ceres

W. Neumann (1,2), D. Breuer (2) and T. Spohn (2)
(1) University of Münster, Münster, Germany, (2) German Aerospace Center, Berlin, Germany (wladimir.neumann@dlr.de/ Fax: +49-30-67055303)

Abstract

Both targets of the Dawn mission – the asteroids Vesta and Ceres represent case studies for the differentiation of the protoplanets that formed in the early solar system and served as building blocks of the planets including Earth. Based on our numerical studies, we compare the process of the differentiation and the internal structure of these bodies.

1. Introduction

Vesta and Ceres, observed closely by Dawn, are both altered remnants of the planetesimals that accreted in the early solar system. Such bodies can be subdivided into rocky objects (that have chondritic bulk composition or are derivates of such bodies, such as asteroids 21 Lutetia and 4 Vesta) and icy ones having composition that contains a substantial amount of water (e.g., carbonaceous chondritic objects, the dwarf planet Ceres, and the icy satellites). Vesta and Ceres are two completely different endmembers formed during the planetesimal differentiation.
Large variation of the surface properties can be observed. For instance, Vesta has a dry, basaltic surface produced by igneous processes (indicating a differentiated structure and resurfacing by lava flows), while Ceres´ surface is characterized by water bearing minerals. There is geochemical evidence for wide-spread silicate melting and even magma oceans on Vesta as well as for ice melting and water-rock differentiation on Ceres.
According to these compositional constraints, the differentiation of these objects from an initially nearly homogeneous interior to the development of a stratified structure took entirely different paths.

2. Models

We developed numerical models to study the formation and evolution of planetesimals, asteroids and dwarf planets[1]. We investigated the influence of porosity, compaction, melting, melt migration and the redistribution of the heat sources on the thermo-chemical evolution of rocky planetesimals by further considering differentiation via porous flow and Stokes flow as well as heat transport by liquid-state convection in crystal-melt mixtures. This work provides constraints on the timing and duration of the core formation and on the formation of a silicate crust. In addition to metal-rock compositions[1,2], models for ice-silicate planetesimals were developed that include water-rock differentiation[3]. These models consider among others ice melting, water-rock differentiation, convection in a water ocean, accretional heating, and hydrothermal convection. The plausible evolution scenarios and interior structures of ice-rich planetesimals depending on their composition, formation time, and accretion duration were explored. The models described were applied to Vesta and Ceres.

3. Vesta

An unprecedented amount of data is available from the howardites, eucrites and diogenites and the Dawn mission and it is widely accepted that Vesta has a metallic core with a radius of approximately half of the asteroid's radius. Therefore, Vesta serves as a case study of melting and differentiation processes in protoplanets. While the HEDs were produced by igneous processes, they can either be products of the early partial melting or residual melts expelled by a crystallizing magma ocean. Isotopic compositions indicate differentiation within the first few Ma after CAIs, while siderophile depletions indicate core formation prior to the crystallization of eucrites and within ≈1-4 Ma after CAIs.
Model calculations show that after the accretion phase, radiogenic heating induced compaction and the associated radius decrease. Early ^{26}Al-rich silicate melt migrated towards the surface causing a strong concentration of ^{26}Al in the sub-surface. Here, the temperature increased rapidly and the melt fraction increased producing a convecting, *O*(1) km thick "shallow" magma ocean. Above the magma ocean, partial melt percolated to the surface forming a basaltic crust. The basaltic crust and the sub-surface are the first differentiated layers. Below this layer, first the iron percolated from the upper mantle

towards the center, then the rest of the mantle and the iron core formed simultaneously. However, no global magma ocean formed in the mantle. Within less than 0.3 Ma the differentiation was completed.
We favor formation of Vesta within 1 Ma after CAIs, because only then the silicate melt can reach the surface and form a crust. An important consequence is the lack of heating in the mantle, which prevents a whole-mantle magma ocean and keeps the melt fractions in the mantle below 50 %. Our results favor the early partial melt origin of the non-cumulate eucrites, while the cumulate eucrites and diogenites form from the partial melt that percolated upwards after the crystallization of the shallow magma ocean, but was not able to reach the surface. The extrusion of the basaltic melt in our calculations is due to porous flow and small-scale shallow dyking. This correlates with the presence of the crust but a lack of distinct volcanic structures on Vesta.

4. Ceres

Because no meteorites have been identified as originating from Ceres, most data comes from the observations by Dawn and from theoretical models. We modeled the compaction of a Ceres-like body that accretes as a porous aggregate, in order to test the hypothesis that Ceres' low density can be explained by a porous interior instead of the presence of ice, and whether compaction occurs due to creep or due to dehydration of hydrated minerals. The porosity change was calculated according to the thermally activated creep flow. We found that compaction of initially porous Ceres is dominated by creep and only slightly perturbed by the dehydration. In particular, dehydration alone cannot lead to compaction because creep can occur before the dehydration. Depending on the accretion timescale, timing of the compaction varies from between a few Ma and more than one Ga. Thereby, late accretion cannot prevent compaction to a porosity of <3%.
Based on the observations by Dawn and assuming a water-rich composition, we calculated water-rock differentiation models assuming 75 vol% rock and 25 vol% ice. We investigated the implications for the presence of liquids and the possibility of cryovolcanism in order to explain surface features observed by Dawn. Accretion times considered cover 1-100 Ma rel. to CAIs. Compaction of the dust pores starts with ice at ≈180-240 K and proceeds with rock minerals at temperatures of up to 730 K. Sub-surface remains too cold to close these pores. The water-rock separation proceeds by water percolation in a rock matrix. Compaction and, therefore, differentiation takes several hundred million years due to a slow temperature increase. Therefore, a water ocean starts forming within 10 Ma after CAIs, but its completion is retarded relative to the melting of ice by up to *O*(0.1 Ga). Convection keeps the ocean cold, counteracts a complete differentiation, and favors retention of a porous undifferentiated crust. Only a thin basal part of the ocean remains liquid until today, while the upper part freezes. Present-day temperatures calculated for a slow accretion (e.g., within >7 Ma) indicate that hydrated salts can be mobile at a depth of ≥5 km implying buoyancy of ice and salt-enriched crustal reservoirs.

5. Discussion

The obvious differences between Vesta and Ceres in the size, density, and composition imply different initial amount of the heat sources, values of the thermal conductivity, melting behavior, and differentiation regime. Higher temperatures are required to produce metallic and silicate melt and to differentiate Vesta completely. For Ceres, moderate temperatures of up to 600 K suffice to melt the water ice and to facilitate differentiation, while there are no indications for melting of metal and silicates in the past. The nature of the differentiation (metal-silicate for Vesta, water-rock for Ceres) necessitates, therefore, different thermal conditions (T>1300 K for Vesta, T>300-600 K for Ceres), and influences strongly the timing of differentiation (0.5 Ma after CAIs for Vesta, *O*(100 Ma) for Ceres) and the final structure (completely differentiated for Vesta vs. partially differentiated for Ceres). Finally, using the observational constraints, the models provide different resulting structures: Vesta is completely compacted and differentiated, with an iron core, a silicate mantle, and a eucritic-diogenitic crust, while Ceres is partially porous and incompletely differentiated, with a rocky core, an ice mantle, and a porous ice-rock crust. Based on the results we extract plausible formation time of 0-1 Ma after CAIs for Vesta and >4-5 Ma after CAIs for Ceres. From the accretion timescale of planetesimals, this points possibly to a formation of Ceres at a larger distance from the sun than its present orbit.

References

[1] Neumann, W., et al., EPSL, 395, 267-280, 2014. [2] Neumann, W., et al., A&A, 584, A117, 2015. [3] Neumann, W., et al., DPS 48 / EPSC 11, 506.08, 2016.

EPSC Abstracts
Vol. 11, EPSC2017-866, 2017
European Planetary Science Congress 2017

The opposition effect on Ceres observed by the Dawn Framing Cameras

S. E. Schröder (1), J.-Y. Li (2), M. Rayman (3), S. Joy (4), C. A. Polanskey (3), U. Carsenty (1), J. C. Castillo-Rogez (3), R. Jaumann (1), L. A. McFadden (5), S. Mottola (1), M. Sykes (2), C. A. Raymond (3) and C. T. Russell (4)
(1) Deutsches Zentrum für Luft- und Raumfahrt (DLR), 12489 Berlin, Germany (stefanus.schroeder@dlr.de), (2) Planetary Science Institute (PSI), Tucson, AZ 85719, U.S.A., (3) Jet Propulsion Laboratory (JPL), California Institute of Technology, Pasadena, CA 91109, U.S.A., (4) Institute of Geophysics and Planetary Physics (IGPP), University of California, Los Angeles, CA 90095-1567, U.S.A., (5) Goddard Space Flight Center (GSFC), Greenbelt, MD 20771, U.S.A.

Abstract

Framing cameras on board the Dawn spacecraft have acquired images of dwarf planet Ceres at near-zero phase angles to study its opposition effect. The opposition geometry was reached through an ingenious scheme of orbital navigation. Images were successfully acquired by both the primary and backup camera in different color bands, reaching near zero phase angle on parts of the surface. Coverage includes the well-known bright area in Occator crater known as Cerealia Facula. Analysis of this rich data set and comparisons with results from laboratory experiments will provide insight into the regolith properties of Ceres and its enigmatic bright terrains.

1. Introduction

The reflectance of planetary regoliths is known to increase dramatically towards zero solar phase angle, a phenomenon known as the "opposition effect". The strength of the opposition effect is governed by two mechanisms, shadow hiding and coherent backscatter, which are related to regolith properties like particle size and morphology, composition, packing density, and surface roughness. The first instance of the opposition effect on a minor body was reported for asteroid Massalia [1]. Resolved images of minor body surfaces at near-zero phase angles are rarely acquired by spacecraft because of the resources required and the risks of spacecraft eclipse on the other side of the body. Often, such images are acquired on approach during a flyby, as for asteroids Steins [2, 3] and Lutetia [4, 5, 6] by Rosetta. Sometimes, the small mass of the body allows the spacecraft to slowly move into the opposition geometry, as for asteroid Itokawa by Hayabusa [7] and comet 67P/Churyumov-Gerasimenko by Rosetta [8]. The lowest phase angle at which Ceres had thus far been observed by ground-based telescopes (unresolved) was 1.1° [9]. The Dawn cameras have now resolved its surface at phase angles smaller than that.

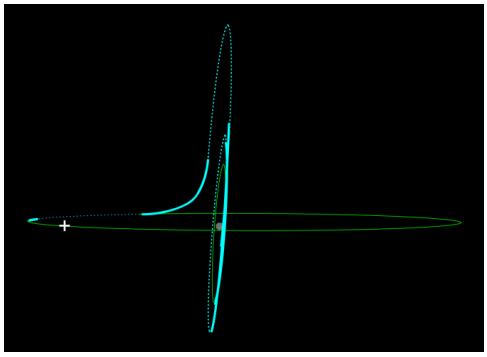

Figure 1: Dawn orbital maneuvers to achieve the opposition geometry (plus sign), with Ceres in the center. Dawn was thrusting in the parts of the orbit drawn in bold.

2. Orbital maneuvers

In a remarkable feat of orbital navigation, Dawn was carefully nudged into the opposition geometry. First, Dawn moved into an elliptical polar orbit, thrusting with its ion engine only in selected parts of the orbit. Then, another thrusting session changed the spacecraft beta angle (the angle between the vector to the Sun and the orbital plane) by almost 90°, achieving the opposition geometry (Fig. 1). A risky eclipse of the spacecraft behind Ceres was avoided by the natural drift of the beta angle due to Ceres' motion in its orbit around the Sun.

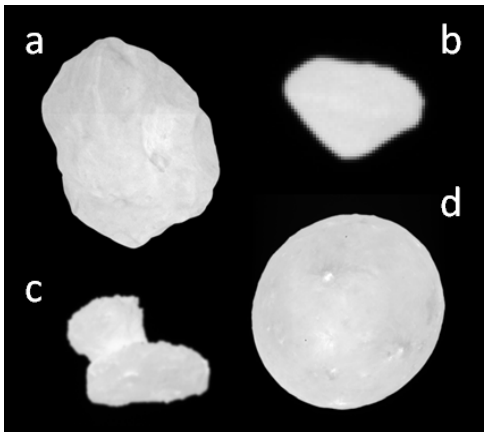

Figure 2: Opposition images of (a) Asteroid Lutetia, (b) asteroid Steins, (c) comet 67P/Churyumov-Gerasimenko, (d) dwarf planet Ceres. Note the absence of any perceptible shadowing, characteristic for images at near-zero phase angle.

3. Data set acquired

Both cameras (FC1 and FC2) were operated during the opposition phase. Images were acquired with four different exposure times every 5 minutes, using the clear filter and five narrow-band filters. We are in the process of validating and calibrating the data. It appears that Dawn reached a geometrical phase angle of zero on the Ceres surface. The effective phase angle of the observations is affected by the finite angular size of the Sun (0.2° at Ceres). For the bright areas inside Occator crater, Cerealia Facula, angles as low as 0.7° were reached. The phase function of Ceres has now been sampled over a range of 155°, the widest available for any minor body. We show a raw image of Ceres in opposition in Fig. 2, together with opposition images of other minor bodies. At first glance, Ceres seems to conform to the relation between strength of the opposition surge and geometric albedo reported by [10], who found that the opposition effect for asteroids of intermediate geometric albedo is stronger than that for asteroids of lower and higher albedo. Special effort will be devoted to analyzing the very bright Faculae, whose photometric properties are very different from Ceres average [11, 12], clues to which we hope to uncover by comparing with the results of photometric experiments.

Acknowledgements

We thank the Dawn flight team for realizing these unique observations.

References

[1] Gehrels, T.: Photometric studies of asteroids. V. The light-curve and phase function of 20 Massalia, ApJ, Vol. 123, pp. 331-338, 1956

[2] Schröder, S. E. et al.: Evidence for surface variegation in Rosetta OSIRIS images of asteroid 2867 Steins, P&SS, Vol. 58, pp. 1107-1115, 2010

[3] Spjuth, S. et al.: Disk-resolved photometry of Asteroid (2867) Steins, Icarus, Vol. 221, pp. 1101-1118, 2012

[4] Masoumzadeh, N. et al.: Photometric analysis of Asteroid (21) Lutetia from Rosetta-OSIRIS images, Icarus, Vol. 257, pp. 239-250, 2015

[5] Schröder, S. E. et al.: Variegation and space weathering on asteroid 21 Lutetia, P&SS, Vol. 117, pp. 236-245, 2015

[6] Hasselmann, P. H. et al.: Asteroid (21) Lutetia: Disk-resolved photometric analysis of Baetica region, Icarus, Vol. 267, pp. 135-153, 2016

[7] Yokota, Y.: Opposition Effect on Itokawa: Preliminary Report from Hayabusa Images, 37th Annual Lunar and Planetary Science Conference, March 13-17, 2006, League City, Texas, abstract no. 2445, 2006

[8] Masoumzadeh, N. et al.: Opposition effect on comet 67P/Churyumov-Gerasimenko using Rosetta-OSIRIS images, A&A, Vol. 599, pp. A11, 2017

[9] Tedesco, E. F. et al.: Worldwide photometry and lightcurve observations of 1 Ceres during the 1975-1976 apparition, Icarus, Vol. 54, pp. 23-29, 1983

[10] Belskaya, I. N. and Shevchenko, V. G.: Opposition Effect of Asteroids, Icarus, Vol. 147, pp. 94-105, 2000

[11] Li, J.-Y. et al.: Surface albedo and spectral variability of Ceres, ApJ Letters, Vol. 817, pp. L22, 2016

[12] Schröder, S. E. et al.: Resolved spectrophotometric properties of the Ceres surface from Dawn Framing Camera images, Icarus, Vol. 228, pp. 201-225, 2017

EPSC Abstracts
Vol. 11, EPSC2017-892, 2017
European Planetary Science Congress 2017

Thermal convection regimes in asteroid (1) Ceres

M.Formisano, C.Federico, M.C. De Sanctis and G. Magni
INAF-IAPS Rome (Italy), Via del Fosso del Cavaliere 100, 000133 (michelangelo.formisano@iaps.inaf.it)

Abstract

Ceres is a "transition body" of the Main Asteroid Belt since it shows some features of the icy satellites of the outer solar system and other peculiarities of the rocky bodies of the inner region. Its surface exhibits evidences of ammoniated phyllosilicates [1] and of water ice [2], for example in craters as Oxo [4][5] or Occator [3]. Probably it formed in an outer (and icy) region of the solar system and then migrated in the current position. The value of the normalized moment of inertia, 0.37 [7], suggests that Ceres is partially differentiated: theoretical models (e.g.[9]) propose a structure made of a rocky core (of about 350 km) and an icy mantle of about 100 km, since the mean density is around 2000 kg m^{-3} [7]. The presence of a heavier crust than the mantle have been hypothesized by [6], in which it was studied the possible overturn of the crust, the energy released by this process and the consequent chemical reprocessing of the crust itself. The crust can also undergo thermal and mechanical stresses due to the presence of active convective cells in the interior layers, which can cause the break or the uplift of the crust. Ahuna mons could be, in this sense, a "product" of the thermal convection in deep interiors [8]. It is an isolated mountain, about 4.5 km high, localized at 10.4° S 316.2° E.

In this work, by using a 2D numerical code based on a finite element method (www.comsol.com) we solve the Navier-Stokes equation coupled with the thermal equation and varying the composition of the convective cell we can study the different thermal convection regimes and their physical consequences.

1. The Model

We numerically solve the Navier-Stokes equations coupled with the thermal equation with the assumption that the density variation is important only in the term of the buoyancy (*Boussinesq approximation*). Neglecting the inertial term, since the Prandtl number is very high in our context, we can write the Navier-Stokes equation as:

$$\rho\frac{\partial\vec{u}}{\partial t} = \vec{\nabla}\cdot\left[-p\vec{I} + \mu\left(\vec{\nabla}u + \left(\vec{\nabla}u\right)^T\right)\right] + F, \quad (1)$$

where F is the bouyancy term that represents the "link" with the heat equation:

$$\rho c_p\frac{\partial T}{\partial t} + \rho c_p\vec{u}\cdot\vec{\nabla}T + K\vec{\nabla}\cdot\vec{\nabla}T = 0. \quad (2)$$

In the above equations u is the convective velocity. We fixed temperature at the bottom (hot) and at the top (cold) of the mantle, with a drop in temperature of 200 K, based on the results of the models found in literature (e.g.[9]). The convective cell (the mantle) is assumed to be 100 km in size. No slip conditions is imposed on all boundaries: this condition requires that the velocity of the fluid tends to zero at wall-fluid interface. All the equations are in the dimensionless form. The mantle is supposed to be made of a mixture of ice and rock.

2 Discussion and Preliminary Results

In Fig.1 we report some preliminary results obtained with our numerical simulations. In the left panel (A) we report the results in the case of 90% of ice and 10% of rock, in the middle panel (B) it is shown a case of pure ice mantle and in the right one (C) the composition is 70% of rock and 30% of ice.

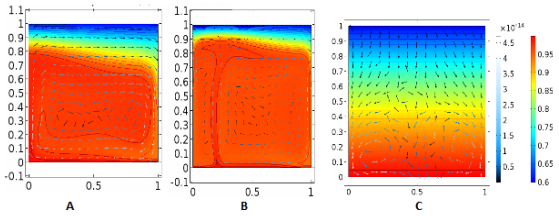

Figure 1: (A) 90% rock & 10% ice; (B) pure ice mantle; (C) 70% rock & 30% ice.

Case A is characterized by a Rayleigh number of the order of 10^7 that lead to a "classical" convective cell, with an isothermal profile and a viscous top layer, identifiable with the crust, of the order of few kilometers. This crust can undergo the thermal/mechanical effects of the convection and eventually break or bulge, depends on the assumed physical parameters. If the composition is pure ice (case B) the Rayleigh number increase of an order of magnitude and in this case we observe the formation of a channel in which material (ice?) from the inside can be expelled to the outside. In case of an important volume percentage of rock (30%), the Rayleigh number (10^5) is not sufficient to trigger the thermal convection.

Acknowledgments

This work is supported by an ASI grant.

References

[1] De Sanctis, M.C., et al. 2015, Nature, 528, 241

[2] Schmidt, B.E.,et al. 2017, Nature Geoscience, 10, 338–343

[3] Nathues, A., et al. 2015, Nature 528, 237–240

[4] Raponi, A., et al. 2017, Lunar and Planetary Science XLVIII (2017)

[5] Combe, J.-P. et al. 2016, Science 353.

[6] Formisano, M., et al., 2016, MNRAS, 463, 1, 520-528

[7] Park, R.S. et al. 2016, Nature, 537, 515-517

[8] Sori, M.M., et al., 2017, Geophysical Research Letters, 44, 3, 1243-1250

[9] Neveu, M. and Desch, S.J., 2015, Geophysical Research Letters, 42, 23, 197–10

EPSC Abstracts
Vol. 11, EPSC2017-920, 2017
European Planetary Science Congress 2017

The Tectonics of Ceres and Vesta

D. L. Buczkowski (1), J. E. C. Scully (2), C. A. Raymond (2), C. T. Russell (3) and the Dawn Science Team
(1) JHU/APL, Maryland USA, (2) JPL, California, USA, (3) UCLA, California, USA (Debra.Buczkowski@jhuapl.edu / Fax: 443-778-8939)

Abstract

Images of Vesta and Ceres taken by the Dawn spacecraft revealed large-scale linear structural features on the surface of both asteroids. We evaluate the morphology of the Vesta and Ceres structures to determine 1) what processes caused them to form and 2) what implications this has for the history of Vesta and Ceres as planetary bodies.

1. Introduction

The Dawn spacecraft [*1*] approached Vesta in July of 2011, left Vesta in late 2012 and went into orbit around Ceres in March 2015. Framing Camera (FC) [2] data from the Approach, Survey, High Altitude Mapping Orbit (HAMO) and Low Altitude Mapping Orbit (LAMO) orbits, including clear filter and color images and digital terrain models derived from stereo images, enabled a three-dimensional characterization of both asteroids.

2. Vesta

2.1 Divalia Fossae

The most prominent set of large linear structures encircle Vesta roughly aligned with the equator. While most of these structures are wide troughs bounded by steep scarps, extending in a similar orientation are muted troughs, grooves and pit crater chains [3]. Fault plane analysis suggests that the formation of the equatorial troughs was triggered by the impact event that formed Rheasilvia basin, as the poles of the planes described by their fault traces cluster on the Rheasilvia central peak [*4*].

The large equatorial troughs encircle approximately 60% of Vesta [3]. Structures with similar orientation (per fault plane analysis [*4*]) are identified in the remainder of the equatorial region. No equatorial troughs cut the topographically high plateau known as Vestalia Terra, but pit crater chains with a similar orientation were identified and proposed to represent sub-surface faulting below the plateau [*3*].

2.2 Saturnalia Fossae

A second set of linear structures on Vesta extend to the northwest from the equatorial troughs [5]. The primary structure in this group extends into the north polar region. In the region north of Vestalia Terra, there are smaller graben and grooves that are parallel to the primary structure [5]. Fault plane analysis ties the formation of the Saturnalia Fossae to Veneneia basin impact event [*4*].

2.3 Brumalia Tholus

As Albalonga Catena, a pit crater chain located in eastern Vestalia Terra, progresses westward it phases from being a topographically low feature of merged pits into being the topographically high Brumalia Tholus, an elongate hill that is evident in both the photographic and topographic data of Vesta [6]. Assuming that Albalonga Catena represents a buried normal fault, it was hypothesized that the topographic high that emerges along its length could have been formed as a magmatic intrusion utilizing the subsurface fracture as a conduit to the surface, intruding into and deforming the rock above it [6].

If a magmatic intrusion, then the core of Brumalia Tholus should be comprised of diogenite, which is a more plutonic rock than the basaltic eucrites and brecciated howardites that have been observed in the equatorial region of Vesta. Teia crater impacts the northern face of Brumalia Tholus and thus its ejecta is likely sampling Brumalia's core material. Analysis by VIR has shown that these Teia ejecta are more diogenitic than other Vestalia Terra materials [6].

3. Ceres

3.1 Samhain Catenae

Kilometer-scale linear structures - including grooves, pit crater chains, fractures and troughs - cross much of the eastern hemisphere of Ceres [7]. Many of these structures appear to be radial to the large craters Urvara and Yalode, and most likely formed due to

impact processes. However, the Samhain Catenae do not have any obvious relationship to impact craters and the lack of raised rims on the merged pits makes it unlikely that these are secondary crater chains. The Samhain Catenae are crosscut by the linear features radial to Urvara and Yalode, indicating they are not fractures formed during those impact events.

Instead, the morphology of these structures more closely resembles that of pit crater chains (buried normal faults). The orientation of the Samhain Catenae relative to each other is suggestive of en echelon fractures. In addition, many of the longer Samhain Catenae are comprised of smaller structures that have linked together; the S-shaped linkages are also suggestive of en echelon fracturing [7].

3.2 Polygonal craters

Polygonal craters, theorized to form when pervasive subsurface fracturing affects crater formation are widespread on Ceres, as they are on icy moons and other asteroids. Those polygonal craters proximal to the Samhain Catenae have straight crater rims aligned with the grooves and troughs. This alignment supports the Samhain Catenae being fracture systems, not ejecta scour or secondary craters [6].

3.3 Floor-fractured craters

Several of the impact craters on Ceres have patterns of fractures on their floors. Geomorphic analyses show that they are similar to lunar floor-fractured craters (FFCs). FFCs on the Moon are hypothesized to be a product of intrusions of magmatic material below the craters uplifting their floors. The Ceres FFCs according to the classification scheme designed for the Moon [8].

Class 1 Ceres FFCs have both radial and concentric fractures at the crater center, and concentric fractures near the crater wall [7]. In the magmatic model these craters represent fully mature magmatic intrusions, with initial doming of the crater center due to laccolith formation resulting in the crater center fractures, while continuing outward uplift of the remaining crater floor results in concentric fracturing adjacent to the crater wall. Other large (>50 km) Ceres FFCs which have only linear or radial fractures at the center of the crater are also classified as Class 1 FFCs [7], but likely represent a less mature magmatic intrusion, with doming of the crater floor but no tabular uplift.

Smaller craters on Ceres are more consistent with Type 4 lunar FFCs [7]. The three Class 4 sub-classes all have a v-shaped moat separating the wall scarp from the crater interior, but different interior morphologies: Class 4a, with both radial and concentric fractures; Class 4b, having a distinct ridge on the interior side of its v-shaped moat and subtle fracturing; Class 4c, with a moat and a hummocky interior, but no obvious fracturing.

A depth vs. diameter analysis shows that, like lunar FFCs, the Ceres FFCs are anomalously shallow [7]. We also observe the d/D trend for the Class 1 FFCs is shallower than that for the Class 4 FFCs. This is consistent with the magmatic intrusion models, which suggest that the increased fracturing of Class 1 FFCs is due to increased uplift.

Acknowledgements

We thank the Dawn Operations team, the Flight team, and the Instrument teams for all their work.

References

[1] Russell, C. T. and Raymond, C. A.: The Dawn mission to Vesta and Ceres, Space Sci. Rev., 163, 3, 2011.

[2] Sierks, H. et al.: The Dawn framing camera. Space Sci. Rev. 163, 263, 2011.

[3] Buczkowski, D.L. et al.: Large-scale troughs on Vesta: A signature of planetary tectonics, Geophys. Res. Lett., doi:10.1029/2012GL052959, 2012.

[4] Jaumann, R. et al.: Vesta's shape and morphology. Science, 336, 687-690, doi:10.1126/science.1219122, 2011.

[5] Scully, J. E. C., et al.: Geomorphology and structural geology of Saturnalia Fossae and adjacent structures in the northern hemisphere of Vesta, ***Icarus,*** doi: 10.1016/ j.icarus.2014.01.013, 2014.

[6] Buczkowski, D.L., et al.: The unique geomorphology and physical properties of the Vestalia Terra plateau, *Icarus*, doi: 10.1016/j.icarus.2014.03.035, 2014.

[7] Buczkowski, D.L., et al.: The geomorphology of Ceres, Science 353, doi: 10.1126/science.aaf4332, 2016.

[8] Jozwiak, L. M., Head, J. W., Wilson, L.: Lunar floor-fractured craters as magmatic intrusions: Geometry, modes of emplacement, associated tectonic and volcanic features, and implications for gravity anomalies. Icarus 248, 424-447, 2015.

EPSC Abstracts
Vol. 11, EPSC2017-929, 2017
European Planetary Science Congress 2017

Origins of Central Pits and Domes on Ceres: Dawn Mapping Constraints and Ganymede Comparisons

P. Schenk (1,2), H.Hiesinger (2), T. Platz (3), T. Bowling (4), B. Schmidt (5), H. Sizemore (6), and the Dawn Science Teams. (1) Lunar and Planetary Institute, Houston Texas, USA (schenk@lpi.usra.edu), (2) Institut für Planetologie, Westfälische Wilhelms-Universität, Münster, Germany, (3) Max Planck Inst. for Solar System Res., Gottingen, Germany, (4) Univ. of Chicago, Chicago, Illinois, USA, (5) Georgia Institute of Technology, Atlanta, Georgia, USA, (6) Planetary Science Institute, Tucson Arizona, USA.

Abstract

The bright faculae and central pit/dome of Occator crater Ceres reveal complex geologic processes on that world and confirm that it is volatile rich. Comparison with domes on Ganymede and terrestrial complex craters but most importantly the observed geologic relations indicate that formation likely involves (hydrothermal?) extrusion of bright material onto the pit floor after its formation during impact, followed by subsequent uplift of the dome, fracturing the carbonate deposits.

1. Introduction

Discovery of a central pit and dome associated with the bright facula at Occator crater on Ceres were unexpected, based on comparison with Saturnian icy moons. These bodies have similar surface gravity and it was thought that if Ceres had an ice-rich crust its craters would resemble those on Saturnian moons. Here we explore the nature of central structures of craters on Ceres and what impact models and comparisons with other bodies tell us.

2. Occator Central Complex

Occator is a very well preserved 93 by 89 km across and ~3.75 km deep [1]. The central structure consists of a circular rounded dome ~2 km wide and ~750 m high (Fig. 1) in the center of a shallow depression ~9 km across and ~1 km deep (Figs. 9, 10). The depression is flanked by high-standing irregularly shaped ridges or massifs that form a partial elevated ring around the depression. This morphology strongly resembles many of the central pit/dome complexes associated with large craters on Ganymede and Callisto [e.g., 2].

The central dome is deeply fractured although the central pit walls are not, suggesting that uplift of the dome surface was responsible and did not involve pit deformation. The fracturing of the bright faculae material also suggests that fracturing may have occurred after bright material emplacement.

Numerical 2-D modeling of impact craters are usually hampered by ambiguities along the central axis of the crater model: i.e., the central structure. Therefore they are of limited use in understanding Occator. Field studies of large terrestrial craters and mapping of central pit and dome craters on Ganymede and Callisto are examined in concert with the Dawn mapping results in an effort to move pit and dome formation forward.

Central structures of terrestrial complex craters are noted for their uplift of deep-seated strata [e.g., 3]. Galileo mapping of central domes and pits was very limited and included no well-resolved examples smaller than ~100 km. Those few domes imaged (Doh [Fig. 2], Neith and Melkart especially) are all deeply fractured [e.g., 2] in a manner reminiscent of Occator. What is lacking on Ganymede is evidence of a residual bright deposit in the manner of Occator. Bright materials are seen in fresh dome craters such as Osiris but these cover the entire crater floor or are more patchy is irregularly distributed, suggesting impact-derived surface frost deposits that erode differentially.

The bright deposit at Occator is partially controlled by local elevation and confined topographically. The ribbon-like nature of the fringes of the Occator deposit (Fig. 1) are consistent with hydrothermal-style outflow from discrete sources leading to carbonate-rich surface deposits [4] that accumulated in the pit floor. These are consistent with numerical models that show the deepest and longest lasting

residual impact heat within the inner core for the crater almost exactly coincident with the location of the central pit.

3. Figures

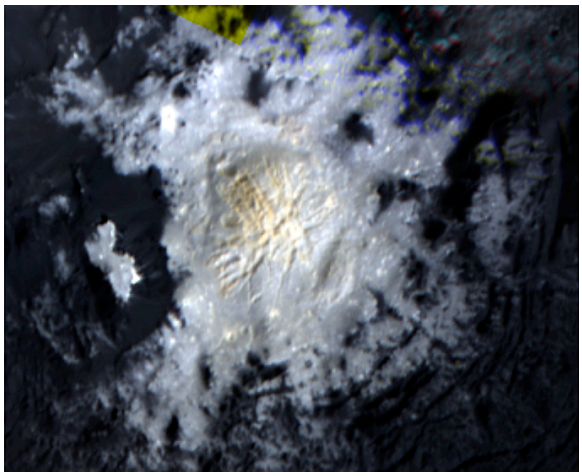

Figure 1: Best color resolution of Occator central structure. Resolution ~35 m/pxl.

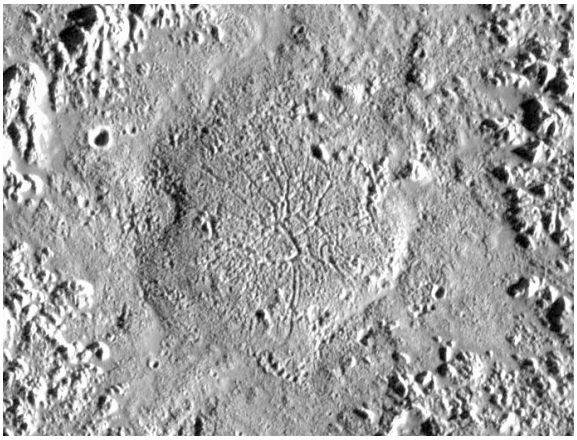

Figure 2: Best Galileo view of fractured central dome: Doh, Callisto. Dome ~25 km across. Res. ~95 m/pxl.

4. Summary and Conclusions

The discovery of complex central structures on Ceres and mapping at high spectral and spatial resolution offers an unexpected opportunity to further constrain these unusual structures. Central pits and domes are confined to ice-rich bodies only. While some central pits are found on Mars, they appear to be distinct and do not possess central domes. While hydrothermal deposition is considered likely in some locations on Mars, we do not observe Occator analogs (perhaps due to the degraded nature of the surface of Mars).

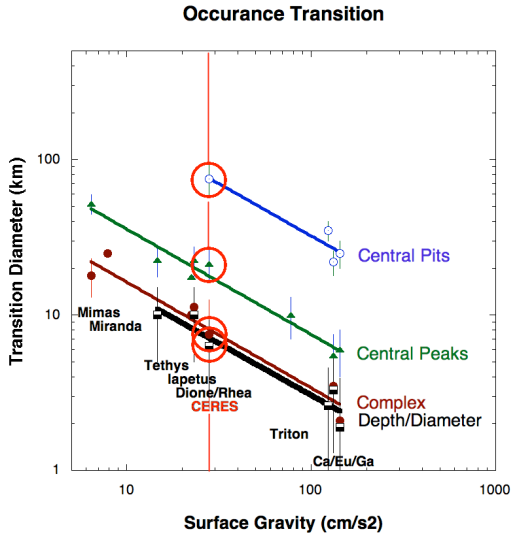

Figure 3: Transition diameters of complex craters on ice-rich bodies. Note lack of transitions to central pits for any of the Saturnian moons, despite nearly identical values for other transitions to Ceres.

The occurrence of central pits on Ceres scales inversely with those on Ganymede, as do other transition diameters such as d/D inflection, central peak formation etc. (Fig. 3), indicative of an outer shell whose rheologic response to impact is controlled by water ice. The lack of such craters in the Saturn system is thus the anomaly and may be related to either the very low temperatures in that system, lower ratios of non-ice materials, or higher impact velocities.

References

[1] Buczkowski, D., et al., Geomorphology of Ceres, *Science*, 353, 1004, 2016.

[2] Schenk, P. et al., 2004, Cratering, in *Jupiter*, Cambridge Univ. Press.

[3] Howard, K, T. Offield and H. Wilshire, Structure of Sierra Madera, Texas, Geol. Soc. Am. Bull., 83, 2795-2808, 1968; Kenkmann, T., Folding within seconds, Geology, 30, 231-235, 2002.

[4] DeSanctis, M., et al., Nature, 536, doi:10.1038/

EPSC Abstracts
Vol. 11, EPSC2017-947, 2017
European Planetary Science Congress 2017

Ceres and Vesta mineralogy determined by VIR on Dawn

M.C. De Sanctis[1] and the Dawn Science Team.

[1]Istituto di Astrofisica e Planetologia Spaziali, INAF, Rome. (mariacristina.desanctis@iaps.inaf.it)

Abstract

The Dawn spacecraft [1] arrived at Ceres in early 2015, the second of its targets, and performed a detailed study of its surface and internal properties. Previously, it performed a detailed orbiting campaign at Vesta. Ceres together with Vesta represent the key to understand some important points relative to the role of the protoplanet size and the water content in determining the evolution of protoplanets and minor bodies. Dawn is equipped with a Visible and InfraRed Mapping Spectrometer (VIR) [2] to study the surface composition of the Dawn targets. Here we report about the main VIR results at Ceres and Vesta.

1. Introduction

VIR is an imaging spectrometer coupling high spectral and spatial resolution in the VIS (0.25-1.0 μm) and IR (0.95-5.0 μm) spectral ranges [2]. VIR acquired data during Approach, Survey, High Altitude Mapping (HAMO) and Low Altitude Mapping (LAMO) orbits that provided very good coverage of the surface of Ceres and Vesta. The bodies' surfaces ware mapped with increasing spatial resolution from Survey (CSS) to LAMO orbits (CSL), but this increase was at the expense of coverage.

2. Result

Ceres

The VIR instrument observed Ceres' surface at different spatial resolutions and revealed a nearly uniform global distribution of surface mineralogy. The average thermally-corrected reflectance spectrum of Ceres (Fig. 1) is almost flat in the spectral region below 2.6 μm, but it shows several bands in the 2.6-4.2 μm wavelength region (Fig. 1), at 2.72, 3.05-3.1, 3.3-3.5, and 3.95 μm. The most prominent is a strong and narrow absorption centred at 2.72-2.73 μm indicative of OH-bearing silicates. The other bands indicate the presence of ammonia bearing species and carbonates [3-7].

Clearly, Ceres experienced extensive water-related processes and chemical differentiation. The surface is mainly composed of a dark and spectrally neutral component (carbon, magnetite), Mg-phyllosilicates, ammoniated clays, carbonates and salts. The observed species suggest endogenous, global-scale aqueous alteration [7].

While mostly uniform at regional scale, Ceres' surface shows small localized areas with different species and/or variations in abundances. Water ice has been detected in localized small patches especially at high latitudes [8] in the North hemisphere but also in a crater not far from the equator in the southern hemisphere [9]. Sodium carbonates have been identified in several areas on the surface, notably in Occator bright faculae [10,4] and many of the bright areas that punctuate the surface of Ceres are compatible with the presence of sodium carbonates. Organic matter has been discovered in several places, most conspicuously in a large area close to Ernutet crater [11]. The signature is associated to aliphatic organics.

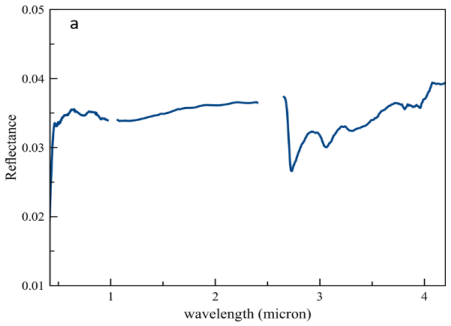

Fig.1 Thermally corrected average spectrum of Ceres in the spectral range 0.4-4.2 μm.

Vesta

Vesta spectra are characterized by pyroxene absorptions at 0.9 and 1.9 μm and spectrally different regions of Vesta have been identified (fig.2). They are characterized by distinctly different band depths, widths, shapes and centers [12], suggestive of different HED lithologies. Although almost all of the surface materials exhibit howardite-like spectra, some large units can be interpreted to be material richer in diogenite (based on pyroxenes band centers) and some others like eucrite-rich howardite units[12,13]. The Rheasilvia basin has its own spectral characteristics: deeper and wider bands, average band centers at shorter wavelengths. These spectral behaviors indicate the presence of Mg-pyroxene-rich (diogenite-rich) terrains in Rheasilvia. Vesta's surface shows considerable diversity at local scales, in terms of spectral reflectance and emission, band depths, centers and spectral slopes. Many bright and dark areas were identified on Vesta from VIR and FC. Bright material is the best example of Vesta endogenous material while dark material is due to contamination by infall carbonaceous chondrites [14,15], also identified as the main carrier of the hydration band at 2.8 micron identified on Vesta. Olivine has been identified on Vesta in different regions [16] and its distribution is compatible with both the main differentiation models (magma ocean and localized plutons).

3. Conclusions

Ceres shows mineralogy and geology dominated by the action of water and other volatile ices mixed with rocks. The surface displays clearly the products of aqueous alteration and ice on the surface [3-11] and subsurface. Moreover, Ceres shows clear sign of "recent" hydrothermal activity [4]. The presence of ammonia in phyllosilicates and salts [3,4,5] indicates the accretion of volatiles, such as ammonia in the original material from which Ceres formed, suggesting a cold formation environment. Moreover, the presence of organic species on Ceres, mixed with minerals formed by water alteration and hydrothermal processes, suggest a favourable environment for the developing of molecules precursor of biological molecules.

Conversely, Vesta shows records of different, less wet, primordial processes that took place at the origin of the solar system. It is basaltic, indicating that internal heat was sufficient to fully differentiate the body, but the surface shows signatures of endogenous OH, delivered by ancient impactors or dust.

Dawn observed two dramatically different objects, relicts of the primordial solar System and prototypes of the terrestrial planets (Vesta) and bodies of the outer solar system (Ceres).

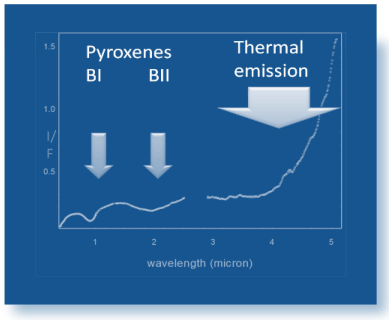

Fig.2 Average Vesta spectrum acquired by VIR.

Acknowledgements

VIR is funded by the Italian Space Agency–ASI and was developed under the leadership of INAF-Istituto di Astrofisica e Planetologia Spaziali, Rome-Italy. The instrument was built by Selex-Galileo, Florence-Italy. The authors acknowledge the support of the Dawn Science, Instrument, and Operations Teams. This work was supported by ASI and NASA. A portion of this work was performed at the JPL/NASA.

References

[1] Russell, C.T. & Raymond, C.A. Space Sci. Rev. 163, 3–23 (2011). [2] De Sanctis et al., SSR, 163, 2011).[3] De Sanctis, M.C. et al., Nature 528, (2015). [4] De Sanctis M.C. et al., Nature , 536, (2016). [5] King et al., Science, (1992).[6] Rivkin, A.S. et al., , Icarus 185, (2006). [7] Ammannto et al. *Science*, 353 aaf4279 (2016). [8] Combe et al., Science, 353, (2016). [9] Raponi et al., in preparation (2017). [10] Carrozzo et al., submitted, (2017). [11] De Sanctis et al., Science, (2017).[12] De Sanctis et al., Science (2012). [13]Ammannito et al., MAPS, (2013). [14] McCord et al., Nature, (2012). [15] De Sanctis et al., ApJLett. (2012). [16]Ammannito et al., Nature, (2013).

EPSC Abstracts
Vol. 11, EPSC2017-956, 2017
European Planetary Science Congress 2017

Spectral analysis of crater central peak material (ccp)

A. Galiano (1,2), E. Palomba (1,3), A. Longobardo (1), M.C. De Sanctis (1), F.G. Carrozzo (1), A. Raponi (1), F. Tosi (1), E. Ammannito (4), C.A. Raymond (5), C.T. Russell (6) and the VIR team.
(1) INAF-IAPS, Rome, Italy (anna.galiano@iaps.inaf.it), (2) Università degli Studi di Roma Tor Vergata, Rome, Italy, (3) ASDC-ASI, Rome, Italy, (4) ASI-URS, Rome, Italy, (5) JPL, California Inst. Tech, Pasadena, CA, USA, (6) UCLA, Los Angeles, CA, USA.

Abstract

The dwarf planet Ceres, the largest and most massive object in the main asteroid belt, is dark and heavily cratered by impacts. The detection of bright spots, especially in the Occator crater, suggested a vertical gradient in Ceres mineralogical composition [1]. Geologic mapping of Ceres enabled the identification of various surface features of interest [2]. Here we focus our attention on the geologic units known as *crater central peak material* (*ccp*). Ccp composes the central peak of several complex craters, probably representative of fresher material coming from the subsurface as a consequence of the impact [3]. We carried out a spectral analysis of ccps found on Ceres to investigate the mineralogical properties of the subsurface material.

1. Introduction

The NASA Dawn mission closely explored Ceres since March 2015. Dawn carries two remote sensing instruments: the *Visible and Infrared mapping spectrometer* (VIR; [4]) and the *Framing Camera* (FC; [5]). The average surface of Ceres is composed by ammoniated (NH_4)-phyllosilicates, Magnesium (Mg)-phyllosilicates, Calcium (Ca) and/or Mg-carbonates, and dark, spectrally featureless material [6]. Bright, widespread areas have been observed on the dwarf planet: the two brightest spots lie in the dome and floor of crater Occator [7] and are referred to as *Cerealia Facula* and *Vinalia Faculae*, respectively. The mineralogical composition of Cerealia Facula is largely different from the rest of Ceres surface, due to the presence of Sodium (Na)-carbonates, Aluminum (Al)-phyllosilicates, ammoniated minerals and dark material [8]. These results, together with the spectral analysis of other bright spots detected by VIR [7] and contrast-rich color mosaics obtained by FC [1], suggest a peculiar composition of the shallow subsurface, different from the average composition observed on the surface. Detailed geologic maps of the dwarf planet have been obtained by using FC images, which allowed the identification of geologic units. To better investigate the possible mineralogical variation in the shallow subsurface, we examined the spectral properties of the geologic unit identified as *crater central peak material* (*ccp*) [2]. This unit is found in the middle of the floor of large craters, and it is supposed to represent shallow subsurface material exposed during the crater formation, after the rebound of the floor and the subsequent creation of a central peak [3].

2. VIR data

To analyse ccps on Ceres, we used hyperspectral data acquired by VIR, i.e. bidimensional spatial images taken in the wavelength range from 0.25 to 5.1 μm. Since the beginning of the mission, Dawn performed several mapping orbits, reducing its altitude from the dwarf planet's surface and acquiring data with increasing spatial resolution. Spectral data from the Survey phase (altitude 4400 km and spatial resolution ~1.1 km/pixel), HAMO phase (altitude 1470 km and spatial resolution 360-400 m/pixel) and LAMO phase (altitude 385 km and spatial resolution 90-110 m/pixel) were used in this work. The photometrically corrected reflectance at 1.2 μm [9] was calculated for the entire dataset.

3. Geologic overview

Central peaks/mounds are topographic features typical of complex impact craters. As consequence of an impact, a shock wave penetrates in the target material, melting and vaporizing the external layer. The shock wave keeps moving below the transient cavity, expelling material (producing ejecta) and ejecting remnants downward (forming the crater floor) or outward (producing crater walls and uplifted crater rim) [10]. To compensate the mass deficit in the transient cavity, the floor begins to uplift [11] and

a central peak may eventually form. Peaks are probably composed of fresher subsurface material, even though the contamination with impact melt deposits cannot be excluded [12].

4. Spectral investigation of ccps

We spectrally investigated 32 ccp units, which stand out in geologic maps of Ceres as they exhibit a different color and morphology with respect to the surrounding floor [2]. We focus our attention on spectral parameters related to Mg-phyllosilicates (2.7 µm band), ammoniated phyllosilicates (3.1 µm band) and carbonates (bands at about 3.4 and 4.0 µm). Band depths and band centers were calculated after continuum removal, whose best fit has been detected in [13]. The goal of this work is to undertake a mineralogical analysis of crater peaks and discriminate a possible differentiation between surface and subsurface. The 2.7- and 3.1-µm band depths are strongly correlated on ccps, being shallower than on the average surface of Ceres (Figure 1). This trend agrees with the general behavior of younger Ceres features [14, 15]. The photometrically corrected reflectance [9] is also considered and compared with spectral parameters to improve the mineralogical analysis. For each ccp unit, we compared the spectral parameters with the crater's floor, to detect a possible contamination of the peak by surrounding material. In this way, we can discriminate the ccp that are most indicative of the Ceres' subsurface material.

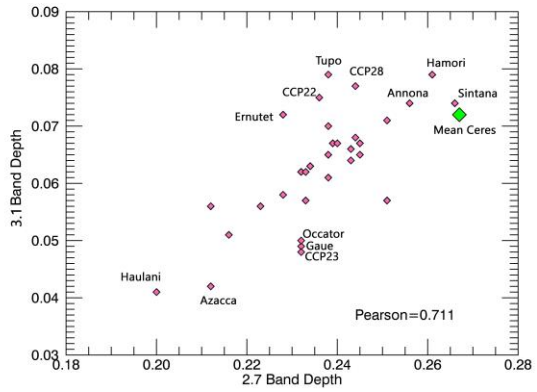

Figure 1: Scatterplot of 3.1 µm band depth in function of 2.7 µm band depth of ccps (pink rhombus) compared with Mean Ceres value (green rhombus).

References

[1] Nathues, A. et al.: FC colour images of dwarf planet Ceres reveal a complicated geological history, Planetary and Space Science, Volume 134, pp. 122-127, 2016.

[2] Mest, S.C. et al.: Geological mapping of the Ac-H-12 Toharu quadrangle of Ceres from NASA's Dawn mission, 47th Lunar and Planetary Science Conference, 21-25 March, The Woodlands, Texas, 2016.

[3] Kuiper, G.P.: On the origin of the lunar surface Features, Proceedings of the National Academy of Sciences of the United States of America, Volume 40, Issue 12, pp. 1096-1112, 1954.

[4] De Sanctis, M.C. et al.: The VIR spectrometer, Space Science Review, Vol. 163, Issue 1-4, pp. 329-369, 2011.

[5] Sierks, H. et al.: The Dawn Framing Camera, Space Science Review, Volume 163, Issue 1-4, pp. 263-327, 2011.

[6] De Sanctis, M.C. et al.: Ammoniated phyllosilicates with a likely outer Solar System origin on (1) Ceres, Nature, Vol. 528, pp. 241-244, 2015.

[7] Palomba, E. et al.: Compositional differences among Bright Spots on the Ceres surface, submitted, 2017.

[8] De Sanctis, M.C. et al.: Bright carbonate deposits as evidence of aqueous alteration on (1) Ceres, Nature, Vol. 536, pp. 54-57, 2016.

[9] Longobardo, A. et al.: EPSC Abstract, 2017.

[10] Croft, S.K.: The excavation stage of basin formation: A qualitative model, In: Schultz, P.H., Merrill, R.B. (Eds.), Multi-ring Basins: Formation and Evolution, Proc. Lunar Planet. Sci., Volume 12A, pp. 207–225, 1981.

[11] Baker, D.M.H. et al.: The formation of peak-ring basins: Working hypotheses and path forward in using observations to constrain models of impact-basin formation, Icarus, Volume 273, pp.146-163, 2016.

[12] Dhingra, D. et al.: Geological mapping of impact melt deposits at lunar complex craters Jackson and Tycho: Morphologic and topographic diversity and relation to the cratering process, Icarus, Volume 283, pp. 268-281, 2017.

[13] Galiano, A. et al.: EPSC Abstract, 2017.

[14] Stephan, K. et al.: An investigation of the bluish material on Ceres, Geophysical Research Letters 44, Issue 4, pp. 1660-1668, 2017.

[15] Palomba, E. et al.: Mineralogical mapping of the Kerwan quadrangle on Ceres, submitted, 2017.

EPSC Abstracts
Vol. 11, EPSC2017-965, 2017
European Planetary Science Congress 2017

Photometry of the Occator faculae on Ceres

A. Longobardo (1), E. Palomba (1,2), M.C. De Sanctis (1), M. Ciarniello (1), A. Galiano (1,3), F. Tosi (1), F.G. Carrozzo (1), A. Raponi (1), M.T. Capria (1,2), F. Zambon (1), E. Ammannito (4), E. Rognini (1), C.A. Raymond (5), C.T. Russell (6)
(1) INAF-IAPS, via Fosso del Cavaliere 100, 00133 Rome, Italy (andrea.longobardo@iaps.inaf.it); (2) ASI-ASDC, Rome, Italy; (3) Università degli studi di Roma Tor Vergata, Rome, Italy (4) ASI-URS, Rome, Italy; (5) JPL-Cal.Tech., Pasadena, California, USA; (6) UCLA, Losa Angeles, CA, USA

Abstract

We study the photometric behavior of reflectance and band depths on the Occator faculae on Ceres and compare it with the Ceres average. The different photometry between Occator and the rest of Ceres indicates that Occator is peculiar not only for the composition, but also for physical properties.

1. Introduction

The NASA/Dawn mission [1] has been orbiting the Ceres asteroid since March 2015, taking hyperspectral images by means of the VIR imaging spectrometer [2], and revealing a homogeneously dark body (reflectance at 0.55 μm and 30° phase is 0.03 [3]), with two very bright faculae located in the Occator crater (10°N 240°E) and reaching a reflectance up to 0.25 [4].
VIR data detected a widespread distribution absorption bands located at 2.7 μm (Mg-phyllosilicates), 3.1 μm (ammonia), 3.4 and 3.9 μm (Mg-carbonates) [5]. However, in some specific locations other carriers could contribute to these bands, e.g. in the Occator crater the 2.7 μm band is caused by Al-phyllosilicates and the 3.4 and 3.9 μm are contributed by Na-carbonates [6]. Moreover, organics could deepen the 3.4 μm band, as in the case of the Ernutet crater [7].
Here we apply a statistical analysis on VIR data aimed at obtaining the behavior of reflectance and band depths with phase angle. In particular, we compare the photometric behavior observed on the Ceres average and on the Occator faculae, respectively, and interpreted the observed differences in terms of optical and physical regolith properties.

2. Method

Retrieval of reflectance and band depth as function of phase angle is based on the approach already used for Vesta [8] and Churyumov-Gerasimenko [9], consisting in a statistical analysis of the dataset. In this case, median values of each spectral parameter at different phase angle bins are retrieved and fitted with a polynomial curve. To better describe the reflectance vs phase angle curve (phase function) we defined two parameters: R30, i.e. the retrieved reflectance at 30° phase angle, and PCS (Phase Curve Slope), i.e. the steepness of the phase function between 20° and 60° phase angle.
In the case of Occator, the analysis was performed only on observations where the 3.9 μm band center is longward of 4 μm, which is a peculiarity of the Occator faculae [6].

3. Results

Albedo. The phase function of the Ceres average shows a low value of R30 and a high one of PCS. The location in the R30-PCS scatterplot is mainly driven by asteroids' taxonomy (Figure 1), and the location of Ceres is consistent with its C-type classification. Contrarily to what expected, the Occator phase function is as steep as the Ceres average one, whereas we should expect a PCS decrease in brighter regions (see the case of Vesta in Figure 1).

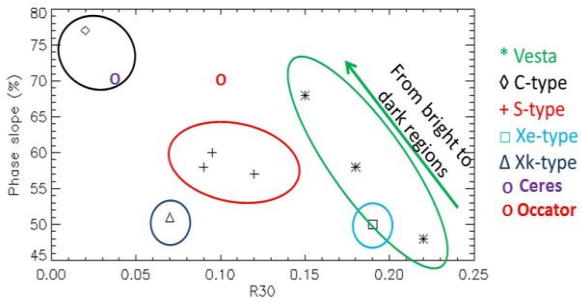

Figure 1: R30 vs PCS scatterplot for Ceres average, Occator and other asteroids [10].

Band depth at 2.7 μm. This band depth linearly increases with phase angle for the Ceres average, which is a common behavior of band depths (e.g. [8]). The increase with phase angle is two times larger for Occator.

Band depth at 3.0 μm. The increase with phase angle of this band is similar for the Ceres average and for Occator, but in the latter case the photometric behavior is strongly uncertain, due to the very weak band in the faculae.

Band depth at 3.4 μm. At increasing phase angle, this band depth increases for the Ceres average.

Band depth at 3.9 μm. This band depth is independent of phase angle for the Ceres average.

4. Conclusions

The obtained results for the Ceres average are somehow expected from its classification and from comparison with other asteroids. The different photometric behaviour of the two carbonate bands could be due to the fact that carriers other than carbonates contribute to the 3.4 μm band.

Different reasons may explain the different photometric behaviour of Occator with respect to the Ceres average:

- *Composition*. Occator includes a larger abundance of bright material (in particular, carbonates) and its carbonates and phyllosilicates are different from the rest of Ceres. However, this does not explain the high PCS, which, according to the Occator R30, should be comparable with S-type asteroids.
- *Granulometry*. A larger regolith grain size would increase PCS and the increase rate of band depth with phase.
- *Roughness*. A larger roughness increases the PCS [9]. In the Occator crater, the roughness increases due to the occurrence of many fractures. Carbonates form at lower topography [11], the observed behaviour of band depth could be affected by the fact that at low phase angles we observe lower heights and hence larger abundance of carbonates.

However, a combination of these hypotheses may occur.

Acknowledgements

VIR is funded by the Italian Space Agency–ASI and was developed under the leadership of INAF-Istituto di Astrofisica e Planetologia Spaziali, Rome-Italy. The instrument was built by Selex-Galileo, Florence-Italy. The authors acknowledge the support of the Dawn Science, Instrument, and Operations Teams.

References

[1] Russell, C.T., et al. (2011). Springer, ISBN: 978-1-4614-4902-7

[2] De Sanctis, M.C. et al. (2011), SSR 163, 329-369

[3] Ciarniello, M. et al. (2016), A&A 583, A31

[4] Palomba, E. et al. (2017), submitted to Icarus

[5] De Sanctis, M.C. et al. (2015), Nature, doi:10.1038/nature16172

[6] De Sanctis, M.C. et al. (2016), Nature, doi:10.1038/nature18290

[7] De Sanctis, M.C. et al. (2017), Science 355, 6326, 719-722

[8] Longobardo, A. et al. (2014), Icarus 240, 20-35

[9] Longobardo, A. et al. (2017), submitted to MNRAS

[10] Longobardo, A. et al. (2016), Icarus 267, 204-216

[11] Stein, N. et al. (2017), submitted to Icarus

EPSC Abstracts
Vol. 11, EPSC2017-966, 2017
European Planetary Science Congress 2017

Elemental composition of Vesta and Ceres

T. H. Prettyman (1), N. Yamashita (1), E. Ammannito (2), N. Schorghofer (1), J. Castillo-Rogez (3), H. Y. McSween (4), M. J. Toplis (5), O. Forni (5), S. Marchi (6), W. C. Feldman (1), B. L. Ehlmann (3, 7), D. J. Lawrence (8), H. G. Sizemore (1), M. D. Rayman (3), C. A. Polanskey (3), S. P. Joy (9), C. A. Raymond (3), C. T. Russell (9)
(1) Planetary Science Institute, USA (prettyman@psi.edu), (2) Italian Space Agency, Italy, (3) NASA Jet Propulsion Laboratory, California Institute of Technology, USA, (4) University of Tennessee, USA, (5) University of Toulouse, IRAP, France, (6) Southwest Research Institute, USA, (7) California Institute of Technology, USA, (8) Johns Hopkins University Applied Physics Laboratory, USA, (9) University of California Los Angeles, USA.

Abstract

Dawn's decade-long journey has provided a close look at the largest objects in the main asteroid belt, Vesta and Ceres. Dawn confirmed many of our hypotheses about Vesta, the putative source of the basaltic, howardite, eucrite and diogenite (HED) meteorites. The unexpected presence of exogenic hydrogen on Vesta and the absence of an olivine signature within the largest impact basin provided further constraints on impact processes and Vesta's geochemical evolution. In contrast to Vesta, Ceres is "wet" and formed beyond the snow line in the solar nebula. Dawn confirmed that Ceres is water rich and showed that Ceres underwent aqueous alteration on a global scale. Here we present measurements of the sub-surface elemental composition of Vesta and Ceres by Dawn's Gamma Ray and Neutron Detector (GRaND) [1]. We describe how elemental measurements constrain the origins and evolution of these largely intact protoplanets.

1. Elemental data

Gamma rays and neutrons are produced by the steady bombardment of the regolith of Vesta and Ceres by galactic cosmic rays. Gamma rays are also made by the decay of long-lived radioelements, K, Th, and U. A portion of the gammas and neutrons escape the surface and are detected by GRaND in orbit. These provide a fingerprint of the elemental composition of the bulk regolith to depths of about a meter.

2. Vesta

The globally-averaged Fe/O, Fe/Si, and K/Th ratios were found to be consistent with the HED meteorites [e.g. 2], providing further indication that Vesta is the HED parent body. The elemental data are consistent with a differentiated planetesimal that accreted inside the snow line from a volatile poor source. Vesta's basaltic regolith contains exogenic hydrogen in the form of hydrated minerals delivered by carbonaceous chondrite impactors [e.g. 2, 3] (Figs. 1A, 1B).

3. Ceres

Hydrated minerals, including OH and ammoniated phyllosilicates, are widespread on Ceres [e.g. 4] (Fig. 1C). Beneath the optical surface, the regolith is H-rich, with equatorial concentrations similar to that of the the aqueously-altered CI chondrites. Excess hydrogen near the poles is probably in the form of water ice, which is stable near the surface at high latitudes [5] (Fig. 1D). Analyses of Fe indicate that Ceres' underwent modest ice-rock fractionation, resulting in a partially differentiated interior [5]. The latest elemental analyses and implications for Ceres' origin and hydrothermal evolution are presented.

References

[1] Prettyman, T. H. et al.: Dawn's Gamma Ray and Neutron Detector, *Space Sci. Rev.*, Vol. 163, pp. 371-459, 2011.

[2] Prettyman T. H. et al.: Elemental mapping by Dawn reveals exogenic H in Vesta's regolith, *Science*, Vol. 338, Issue 6104, pp. 242-246, 2012.

[3] De Sanctis, M. C. et al.: Detection of Widespread Hydrated Materials on Vesta by the VIR Imaging Spectrometer on Board the Dawn Mission, *Astrophys. J. Lett.*, Vol. 758, L36, 2012.

[4] Ammannito, E. et al.: Distribution of phyllosilicates on the surface of Ceres, *Science*, Vol. 353, aaf4279, 2016.

[5] Prettyman, T. H. et al.: Extensive water ice within Ceres' aqueously altered regolith: Evidence from nuclear spectroscopy, *Science*, Vol. 355, Issue 6320, pp. 55-59, 2017.

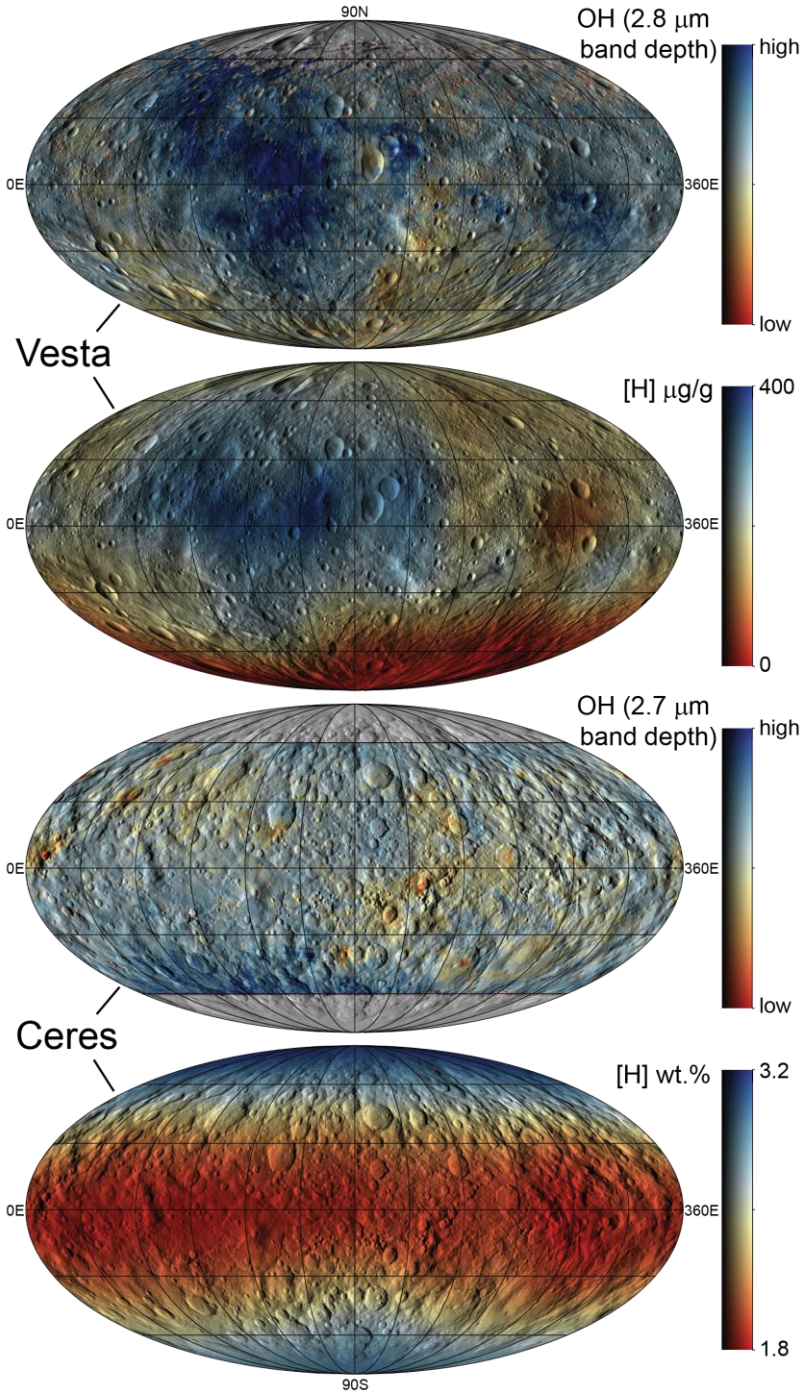

Figure 1.

(Data superimposed on shaded relief)

A. Map of 2.8 μm absorption band by Dawn's Visible and Infrared Mapping Spectrometer (VIR) gives the distribution of hydroxyl (OH) on Vesta's surface [3].

B. Distribution of hydrogen determined within the top meter of Vesta's surface, determined by neutron spectroscopy (GRaND) [2].

C. Distribution of hydrated minerals on Ceres' surface (VIR) [4].

D. Distribution of hydrogen within the top meter of Ceres' surface, deterined by neutron spectroscopy (GRaND) [5].